DESIGN OF A STYLUS WITH VARIABLE TIP COMPLIANCE

by

ÖZDEMİR CAN KARA

Submitted to
the Graduate School of Engineering and Natural Sciences
in partial fulfillment of
the requirements for the degree of
Master of Science

SABANCI UNIVERSITY

August 2018

DESIGN OF A STYLUS WITH VARIABLE TIP COMPLIANCE

APPROVED BY:

Assoc. Prof. Dr. Volkan Patoğlu
(Thesis Supervisor) .....

Asst. Prof. Dr. Bekir Bediz .....

Assoc. Prof. Dr. Mehmet İsmet Can Dede .....

DATE OF APPROVAL: 13.08.2018

ABSTRACT

DESIGN OF A STYLUS WITH VARIABLE TIP COMPLIANCE

ÖZDEMİR CAN KARA

Mechatronics Engineering M.Sc. Thesis, August 2018

Thesis Supervisor: Assoc. Prof. Volkan Patoglu

Keywords: Physical human-robot interaction (pHRI), physical impedance modulation, compliant mechanisms, negative stiffness, pseudo rigid body modeling

Humans are known to modulate the impedance properties of their fingers in order to physically interact with the environment. For instance, painting or palpating fragile objects require high compliance of the fingers, while writing and measuring entails high precision position control, for which the stiffness of the fingers is increased considerably.

In this thesis, we present the design, modeling, implementation, characterization and user verification of a stylus with variable tip compliance. In particular, we propose a variable stiffness mechanism as a compliant stylus that features an adjustable tip stiffness such that users can modulate compliance as needed to match the requirements of the task they perform.

The variable stiffness of the stylus tip is achieved through transverse stiffness variations of axially loaded beams around their critical buckling load. Integrating an axially loaded beam with a compliant transmission mechanism, the stylus tip stiffness can be modulated over a large range. In particular, very low stiffness levels can be rendered with high fidelity, without sacrificing the mechanical integrity and load bearing capacity of the stylus.

Compliant transmission mechanism of the stylus is analyzed through pseudo rigid body modeling which is a convenient and efficient way of modeling flexible elements exhibiting non-linear characteristics under large deflections. Furthermore, a novel pseudo rigid body model for a fixed-guided buckling beam that captures the

transverse stiffness variations around the first critical buckling load is proposed and verified. These models are integrated to derive a lumped parameter model of the compliant stylus with adjustable tip stiffness. The lumped parameter model due to pseudo rigid body modeling promotes ease of analysis for design, by hiding the underlying modeling complexities of continuum mechanics from the designer.

We provide experimental characterization results detailing the range of stiffness modulation achieved with several prototypes and verifying the accuracy of the equivalent pseudo rigid body model. We also present a set of human subject experiments that provide evidence in establishing the efficacy of the modulated stylus stiffness on the human performance.

ÖZET

DEĞİŞTİRİLEBİLİR UÇ ESNEKLİĞİNE SAHİP STYLUS TASARIMI

ÖZDEMİR CAN KARA

Mekatronik Mühendisliği Yüksek Lisans Tezi, Ağustos 2018

Tez Danışmanı: Doç. Dr. Volkan Patoğlu

Anahtar Kelimeler: Fiziksel insan-robot etkileşimi, fiziksel empedans modülasyonu, esnek mekanizmalar, negatif sertlik, sahte rijit cisim modelleme

İnsanların, çevreleriyle fiziksel olarak etkileşime girmek için parmaklarının empedans özelliklerini kontrol ettikleri bilinmektedir. Örneğin, boyama ya da kırılgan nesnelerle etkileşim parmakların yüksek esnekliğini gerektirirken, yazma parmakların sertliğinin önemli ölçüde arttırıldığı yüksek hassasiyetli pozisyon kontrolünü gerektirir.

Bu tezde, değişken uç esnekliğine sahip bir stylus tasarımı, modellemesi, uygulanması, karakterizasyonu ve kullanıcı doğrulaması sunulmaktadır. Kullanıcıların gerçekleştirdikleri görevin gereksinimlerini karşılamak için, cihaz esnekliğini gerekli seviyede modüle edebileceği ayarlanabilir uç sertliğine sahip bir stylus olarak kullanılabilen, değişken esnekliğe sahip bir mekanizma önerilmiştir.

Stylus ucunun değişken esnekliği, kritik burkulma yüklerinin etrafında eksenel olarak yüklenmiş kirişlerin enine sertlik varyasyonları ile elde edilmiştir. Eksenel olarak yüklenmiş bir kirişin esnek bir aktarma mekanizması ile bütünleştirilmesi sonucu stylus ucunun esnekliği geniş bir aralıkta ayarlanabilmektedir. Özellikle, çok yüksek esneklik seviyeleri, stylusun mekanik bütünlüğünden ve yük taşıma kapasitesinden ödün vermeden, yüksek doğrulukla elde edilebilmektedir.

Stylusun esnek güç iletim mekanizması, büyük sapmalar altında lineer olmayan özellikler sergileyen esnek elemanların analizi uygun ve etkili bir yolu olan sahte rijit cisim modellemesi yoluyla analiz edilmiştir. Ayrıca, birinci kritik burkulma yükü etrafındaki enine rijitlik değişimlerini kapsayan bir ucu sabit diğer ucu kayar mesnetli burkulma kirişi için yeni bir sahte rijit cisim modeli önerilmiş ve doğrulanmıştır. Bu

modeller, ayarlanabilir uç esnekliğine sahip stylusun yuvarlanmış parametre modelini elde etmek için bir araya getirilmiştir. Sahte rijit cisim modellemesine bağlı yuvarlanmış parametre modeli, tasarımın analizini kolaylaştırarak, sürekli ortamlar mekaniğinin altında yatan modelleme karışıklıklarını tasarımcıdan saklaması nedeniyle tercih edilmektedir.

Çeşitli prototipler ile elde edilen esneklik değişim aralığını ve eşdeğer sahte rijit cisim modelinin doğruluğunu teyit eden deneysel karakterizasyon sonuçları sunulmuştur. Ayrıca, farklı stylus sertliklerinin insan performansı üzerindeki etkinliğini ortaya koyan bir dizi insanlı deneylere yer verilmiştir.

≪ To my beloved family ≫

ACKNOWLEDGEMENTS

First I would like to express my sincere gratitude to my thesis supervisor Assoc. Prof. Volkan Patoğlu for the useful comments, remarks and engagement through the learning process of this master thesis. Not only his knowledge, attention to detail and work ethic but also his support, trust and understanding helped me a great deal in the path of becoming a good researcher.

For this thesis I would like to thank my committee members: Asst. Prof. Bekir Bediz and Assoc. Prof. Mehmet İsmet Can Dede for their time, interest, participation, insightful questions and helpful comments.

I would also like to warmly thank Assoc. Prof. Ahmet Onat and Assoc. Prof. Kemalettin Erbatur for the help, the insights and the comments he gave me without restraint and also Prof. Dr. Asif Sabanovic, from whose courses and wise words I have learned so much throughout the course of my university studies.

I want to thank Ata Otaran, Yusuf Mert Şentürk, Wisdom Chukwunwike Agboh, Gökhan Alcan and Vahid Tavakol for their friendship and support during extensive hours we have spent studying together. I also want to thank the doctoral student friends from Human Machine Interaction laboratory; Mustafa Yalçın and Gökay Çoruhlu especially for their helpful and constructive at many instances I have faced issues with hardware or software.

I would like to acknowledge the funding support from Sabanci University and The Scientific & Technological Research Council of Turkey (TÜBİTAK) grant 115M698 for my projects that made this thesis, degree and possible.

I owe a special thank to my dearest girlfriend and my best friend, Aysun Mutlu for unfailing support and sacrifice during every moment that we share. Without her help, it became more difficult to overcome hard times of graduate studies period.

Last but foremost I want to thank my family for their constant, unparalleled love, support and understanding that allowed me to continue my education in a successful manner. I am forever indebted to my parents for giving me the opportunities and experiences that have made me who I am. My parents, Özcan and Ayşe Kara raised

me to be an ethical, curious person and always supported my education sparing no sacrifice. My little brother Özgür Kara is the joy of our family and the person that I hope to set a good example in future. I am glad to have them in my life.

Table of Contents

List of Figures

List of Tables

Nomenclature

$2R$	Transverse loading
D	Transverse displacement of the buckling beam
E	Elastic modulus
F_a	Axial load exerted by the actuator on the buckling beam
F_c	Applied force on the compressive spring
F_c	Applied force on the cross flexure joint along the n_1 axis
F_p	Applied force on the parallelogram joint along the n_1 axis
F_{tip}	Applied force on the tip
I	Area moment of inertia
K	Equivalent actuator stiffness
K_f	Stiffness coefficient for pseudo rigid body modeling
K_Θ	Torsional spring constant
K_{cb}	Equivalent actuator stiffness
K_{cub}	Overall cubic stiffness term
K_{lin}	Overall linear stiffness term
K_{ln}	Equivalent actuator stiffness

K_{p1}	Equivalent stiffness coefficient of the 1st parallelogram joint
K_{p2}	Equivalent stiffness coefficient of the 3st parallelogram joint
K_{p3}	Equivalent stiffness coefficient of the prevention parallelogram joint
$K_{p_{eq}}$	Equivalent linear spring constant
K_p	Equivalent linear stiffness of the prevention parallelogram joint
K_s	Stiffness of the compression spring
$K_{t_{eq}}$	Equivalent torsional spring constant
L	Full length of the buckling beam
L_B	Half length of the buckling beam
P	Axial load
P_{cr}	First critical buckling load
S_y	Yield strength
Δ_p	Axial displacement of the adjustable end of the pre-tension spring
Φ_{max}	Maximum deflection of the cross flexure joint
Θ_b	Angle between the tangent of the beam at s and n_1
Θ_n	Rotation angle of the cross flexure joints n=1,2
Θ_p	Rotation angle between n_1 axis and deflected beams
β_n	Rotation angle of the equivalent cross flexure joints n=1,2
δ	Sum of the axial displacement of beam and the transverse deformation of middle of the beam
γ	Characteristic radius factor
μ	Ratio between actuator stiffness and the axial stiffness of the buckling beam

ψ	Half angle between two beams of the cross flexure joint
h	Length of the lever
h_f	Fixed length of the cross flexure joint beam
h_m	Moving length of the cross flexure joint beam
k_c	Cubic stiffness of the buckling beam
k_l	Linear stiffness of the buckling beam
k_{cr}	Equivalent stiffness of the cross flexure joint
k_{p1}	Torsional stiffness coefficient of the 1st parallelogram joint
k_{p2}	Torsional stiffness coefficient of the 2st parallelogram joint
k_{p3}	Torsional stiffness coefficient of the prevention parallelogram joint
l_p	Beam length of the parallelogram joint
n	Proportion of the moving part to total length of the cross flexure joint
s	Path length along the deflected beam
s_n	Displacements of the parallelogram joints n=1,2
t	Thickness of the beam
x	Axial position
x_p	Linear displacement of the parallelogram within the n_1 axis
y	Transverse position

Chapter 1

Introduction

Stylus is originated from Latin word 'stilus', which means a pen shaped instrument to be used for writing on wax tablets. Today, the utilization of styli has been increasing as touch screens and haptic interfaces become ubiquitous. Styli are commonly employed for pointing, navigating, writing, drawing, painting, indenting and measuring on touch screens, as well as for palpating and probing stiffness of tissues to detect their abnormalities in medical applications. Drawing with a stylus can provide better feel rather than drawing with fingertip, since the stylus mimics the natural hand position with a pen and provides better control at drawing applications.

During physical interactions with the environment such as touching different surfaces, gripping and holding objects, humans are known to modulate impedance properties of their limbs. For instance, writing and measuring necessitate highly accurate position control for which the stiffness of the fingers is increased considerably, whereas stiffness of the fingers is lowered for task such as painting or palpating soft-/fragile objects. Therefore, tools that have variable stiffness promise to be effective at tasks where human interacts with the environment, as variable stiffness property not only can help ensure the completion of desired task with more precision, but also may improve the adaptability of the tool for different environments. Moreover,

variable stiffness tools are known to be advantageous for ensuring safety, improving stability, dynamic performance and energy efficiency of interaction tasks. There exists strong evidence in the literature that during tool use representations of the body expand to include "external" object that is being held [4]. Along these lines, several studies [5–8] provide evidence that prostheses with stiffness modulation can improve the performance of an amputee, when the impedance of the prosthesis is matched with the requirements of the task. These studies indicate that the physical properties of any tool that acts as an extension of the body are important and properly matched tool impedance can significantly improve task performance.

In this study, we propose a compliant stylus that features a manually variable tip stiffness such that the users can adjust the stylus compliance as needed to match the requirements of the task they perform. Variable stiffness of the stylus tip is achieved through transverse stiffness variations of axially loaded beams around their critical buckling load. Through integrating an axially loaded beam with a compliant mechanism, we show that the stiffness of the stylus tip can be modulated over a large range that includes very low stiffness levels. In particular, the tip stiffness of the stylus can be modulated (i) by application of the axial compressive loading to increase tip compliance and (ii) by application of tensile axial loading to increase the tip stiffness. The compliant design of the variable stiffness stylus possesses many advantages, such as high precision, absence of friction, stiction, wear and backlash that enable ease of miniaturization. We derive a model for tip stiffness through pseudo rigid body analysis of the underlying compliant mechanism and the buckling beam around its buckling load, and verify these models through experiments. We also provide experimental results detailing range of stiffness modulation achieved with a prototype. Finally, we report results from human subject experiments that provide evidence on the effectiveness of variable stiffness stylus on the human performance.

1.1 Contributions

The main contributions of this thesis can be summarized as follows:

- A novel compliant stylus with manually adjustable tip stiffness is proposed and designed.

  The design can assume a large range of tip stiffness values to match with the requirements of various tasks. In particular, in addition to very high tip stiffness levels, very low stylus tip stiffness levels have been achieved without sacrificing the mechanical integrity and load bearing capacity of the stylus, thanks to the proposed design based on negative stiffness characteristics of the buckling beam.

  The design inherits the advantages of compliant mechanisms. In particular, absence of parasitic effects such as friction, stiction, wear and backlash enables high fidelity stiffness rendering, good agreement with the analytical model, and ease of miniaturization.

  Manual adjustment is preferred for a low cost, easy to use design. The design allows for actuation to be added to the system through the tensioning mechanism; however, electronic components and the controller add some additional complexity.

- A pseudo rigid body model for the compliant stylus with manually adjustable tip stiffness is derived.

  A novel pseudo rigid body model is proposed for fixed-guided beams that captures their transverse stiffness change around their first critical bucking load. The proposed model is based on the analytical solution of buckling beams and has been experimentally verified.

  Modeling the stiffness changes of fixed-guided beams in a lumped parameter model, the proposed model is integrated with the pseudo rigid body of the

compliant transmission mechanism to derive a lumped parameter model of the compliant stylus with manually adjustable tip stiffness. The lumped parameter model proposed by pseudo rigid body modeling promote ease of design by hiding the underlying modeling complexities of continuum mechanics from the designer.

- Several prototypes of compliant stylus with manually adjustable tip stiffness have been implemented and characterized.

  The prototypes have been experimentally characterized and verified to possess a large stiffness range that can achieve an order of magnitude change in the tip stiffness, while being capable of rendering very compliant tips (as low as 0.07 N/mm). Furthermore, excellent agreement (RMS errors less than 3%) between the stiffness characteristics of the prototypes and the predictions based on the proposed analytical stiffness model have been observed.

- The efficacy of the manually modulated stylus stiffness on the human performance has been verified through human subject experiments.

  A set of human subject experiments are designed and performed, where effect of tip stiffness on various tasks are tested. The experimental protocol, the performance metrics and statistical analysis of outcomes are presented.

1.2 Outline

This thesis addresses to design, fabrication, (pseudo rigid body) modelling and implementation of a variable stiffness stylus. In addition, performance evaluation of the design is completed through a set of human subject experiments.

The rest of the thesis is organized as follows:

Chapter 2 presents the literature survey and the background related to styli, pseudo rigid body model, and variable stiffness actuation.

Chapter 3 details the design objectives, the proposed solution and mechanical design of the stylus with manually adjustable tip compliance.

In **Chapter 4**, elaborative kinematic analysis and equivalent pseudo rigid body modelling of the stylus are presented. The stiffness analysis of each compliant elements are explained and the final stiffness equation is formally derived.

In **Chapter 5**, an equivalent pseudo rigid body model for a beam under buckling conditions is investigated and a mathematical formulation of this pseudo rigid body model is derived. The model is also experimentally verified.

Chapter 6 details the prototype and the experimental setup, presents each components of mechanical design and their properties together with the characterization results for the prototype.

In **Chapter 7**, a set of human subject experiments are presented to evaluate the efficacy of the manually modulated stylus stiffness on the human performance. In particular, various tasks demanding different levels of stiffness levels are designed and the experimental protocol and the performance metrics are explained. Finally, the performance evaluations are presented and the outcomes are discussed.

The thesis is concluded with a summary of contributions and a discussion of future works in **Chapter 8**.

Chapter 2

Literature Review

In this section, we review the related works on styli based interactions, pseudo rigid body modelling of compliant mechanisms, various approaches to impedance modulation, and situate this study with respect to the literature.

2.1 Application Areas

Stylus based interactions are commonly used on two applications where a stylus is used as a hand-held pen or as a palpation probe.

2.1.1 Hand-Held Styli

In recent years, several studies have been conducted to enrich and improve stylus based interactions. In most of these studies, vibro-tactile feedback is implemented to add a new modality of interaction. Haptic Pen [9] provides tactile sensations via a push type solenoid actuator aligned with the stylus body to act as an actuated mass. A similar arrangement is used in [10] together with a pressure sensor. SenStylus [11] utilizes two independently controlled rumble vibrators to provide vibration feedback

with a larger spectrum of vibro-tactile effects. Ubi-Pen [12] provides vibration feedback by a pancake type vibrating motor, while also featuring a 3x3 tactile pin array of ultrasonic linear motors to convey texture information to the user. wUbi-Pen [13] is an untethered version of Ubi-Pen, which utilizes an impact generator to create vibration feedback through a wireless controller. This version drops the tactile pin array for simplicity and compactness. HaptiStylus [14] locates two vibration motors at the two opposing ends of the stylus, such that tactile effects based on apparent tactile motion illusion can be delivered. This device also integrates a DC motor to provide rotational torque effects. Finally, Real Pen [15] relies on a linear resonate actuator to deliver tactile and auditory feedback to match friction induced oscillations recorded between the stylus tip and a surface.

Other styli rely on different methods to provide haptic sensations. Among these, Impact [16] proposes a retractable stylus that employs DC motor actuated rack and pinion mechanism to drive a concentric shaft. Force feedback is provided by locking the mechanism at a certain length such that rigid contact takes place. Haptylus [17] improves on retractable stylus idea with the inclusion of a pressure sensor to control the amount of retraction. Furthermore, a voice coil actuator is added to the stylus for vibration feedback. Ungrounded kinesthetic feedback is provided in [18], where three DC motors wind/unwind strings to translate/rotate the tip portion of the stylus with respect to its other end, such that three degree of freedom motion of the tip results in kinesthetic sensations at the hand. Feedback based on dynamic friction with the contact surface is provided in [19] through an electromagnetic coil modulating the friction on a ball rolling at the tip of the stylus. Similarly, a gripping mechanism is proposed in [20] to control the friction on a ball rolling at the tip. Another method is to utilize skin stretch as a haptic feedback. It is provided naturally through daily interaction with the objects. Stylus based skin stretch device is presented in [21] where friction between the moving tactor and the skin surface creates haptic feedback during interaction.

Finally, Elastylus [22] is a non-actuated stylus that adds a spring along its longitudinal axis to provide tip compliance. To the best of authors' knowledge, none of the haptic stylus in the literate allow for modulation of its tip stiffness.

2.1.2 Palpation Probes

Stylus based tools can also be used as palpation probes or indentation apparatus employed during measurement and modeling of tissue properties. For instance, an indentation device for the measurement of cartilage stiffness has been developed in [23], where the interaction force is related to bending of a beam that contacts with the tissue. In [24], a hand held compliance probe is proposed to obtain stress-strain data from different tissues, where the force response is sensed through a load cell. Tempest 1-D [25] is proposed as an instrument for investigation of the viscoelastic properties of soft tissues under small deformations. This instrument consists of a voice coil actuator to excite and a force sensor to measure the stiffness response of tissues. A hand held soft tissue stiffness meter is proposed in [26] that examines stiffness through relationship between resistance of a tissue under constant displacement, where the instantaneous applied force is sensed by an indenter force transducer. In [27], an optical fiber based rolling indentation probe is proposed to measure the soft tissue stiffness distribution. Helical cut sensing structure of this design possesses a spring like behavior with high axial stiffness. When an axial force is applied, the spring like element is compressed and applied axial force is estimated according to the displacement. In [28] a haptic palpation probe is implemented to locate subcutaneous blood vessels during minimally invasive surgery. Tip deflections are measured with a hall effect sensor and applied force is estimated based on the tip deflections and with respect to a spring attached to the end effector.

Apart from the force sensing probes, [29, 30] utilize the measurement of a resonance frequency shift during indentation in order to provide tactile feedback. Work described in [31] presents a palpation probe that consists of tactile sensor array to examine contact impedance through controlling pressure on each sensor element.

None of these probes allow for modulation of its tip stiffness. A probe with variable stiffness has been developed in Sornkarn [32]. In particular, this design is a two degree of freedom controllable stiffness probe proposed to examine the affects of different variables for the accurate estimation of depth during stiff inclusions. The stiffness of the probe can be varied through antagonistic arrangement of two nonlinear springs located inside spring chambers. Similarly, a variable stiffness robotic probe based on a lever mechanism for abdominal tissue palpation is proposed [33]. Our proposed stylus design is significantly different from these two probes at its relies on negative stiffness characteristics of buckling beams to modulate its stiffness and possesses a fully compliant design. Consequently, the proposed design can eliminate the parasitic effects of friction and stiction, can be easily miniaturized and has a very large stiffness rendering range.

2.2 Pseudo Rigid Body Modelling

A compliant mechanism obtains some or all of its motion from the deflection of flexible members. Compliant mechanisms exhibit many advantages, such as elimination of wear, backlash, pin joint associated clearances, need for lubrication and reduction in manufacturing/assembly time and weight. However, modeling compliant mechanisms is more complicated due to the continuum mechanics and non-linearities that dominate their analysis under large deflections. In the literature, multiple methods have been proposed to model compliant mechanism undergoing large deflections. For simple compliant elements, one of these methods is to solve a second order, non-linear differential Bernoulli- Euler equation, which states that the bending moment on the beam is proportional to its curvature, using elliptic integrals of first and second kind [34–37]. Although elliptic integral approach can result in a closed form solution, it is burdensome and difficult to use. Furthermore, this modeling approach is limited to simple compliant elements with certain geometries and loading conditions.

Another widely used method is to employ numerical methods, such as non-linear finite element analysis. Finite element methods (FEM) can solve a wide variety of problems with complex geometries and loading conditions, and calculate approximate solutions with high precision [38, 39]. However, FEM cannot generate a general closed-form solution, which would permit one to examine system response to changes in various parameters. Furthermore, proper selection of element types and appropriate meshing are critical for limiting inherent errors in FEM. Along these lines, user errors while selecting of proper parameters for analysis may lead to fatal errors.

The third alternative, pseudo rigid body modeling, is a simple method to model compliant mechanisms when they undergo large deflection leading to non-linear behavior. This model utilizes equivalent rigid body components that have similar force-deflection characteristics with the flexible members [40, 41]. In other words,

compliant mechanisms are considered as equivalent rigid body mechanisms with certain characteristic compliance. Pseudo rigid modeling has several advantages, including simplicity, ease of use, efficiency, in addition to the high accuracy. Furthermore, as it provides parameterized models, pseudo rigid modeling is suitable for design and optimization problems and can significantly speed up calculations but utilization of pseudo rigid modeling is restricted to structures with regular geometry such as beams with constant cross sectional area. Pseudo rigid body models have been derived for a large range of compliant elements, including flexural pivots, cantilever beams with a force at the free end, beams with fixed-pinned and fixed-guided boundary conditions and initially curved cantilever beams with various boundary conditions [1].

In the literature, fixed-guided beams have received attention in various applications, such as design of a pressure sensor [42], a compliant gripper [43], a compliant parallel guiding mechanism [44–46], a compliant double parallel four-bar mechanism [47], a statically balanced compliant mechanisms [48], a self-retracting fully compliant bistable micro-mechanism [49], an end effector for micro-scribing [50], and a compound compliant parallelogram mechanisms [51].

Generalized analytical closed form solutions does not exist for fixed-guided beams. In the literature, Ma et al. [52] have suggested beam constraint model (Bi-BCM), an extension of the Euler-Bernoulli beam theory, to derive a parametric closed form model for fixed-guided beams. Other than this extended semi-analytical solution, various pseudo rigid body models have been proposed for the analysis of fixed-guided beams. Howell [1] has introduced a simplified model that consists of three links with two pin joints, each joint equipped with torsional springs, as depicted in Figure 2.1.

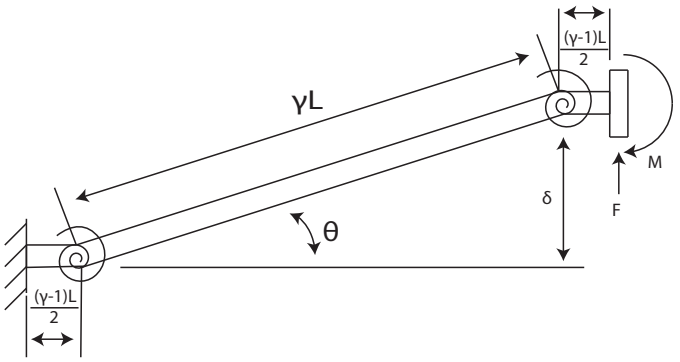

FIGURE 2.1: Fixed-guided beam model proposed by Howell [1]

Lyon et al. [53] have extended the model proposed by Howell [1] to cover various beam end angle values. Based on these works, Midha et al. [2] have proposed a model that analyzes the fixed-guided compliant beams with an inflection point that are subjected to different end moment and force conditions, as presented in Figure 2.2. The location of the inflection point depends on the loading.

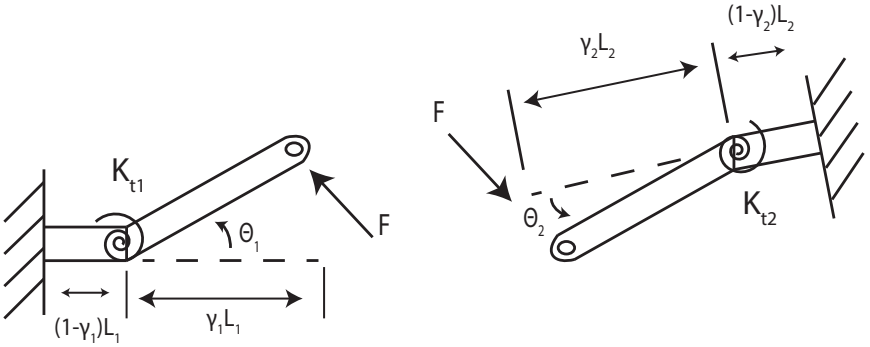

FIGURE 2.2: Fixed-guided beam model with inflection point proposed in [2]

Although all of these models serve as reliable approximations for certain applications, these models focus on the bending deformations and cannot capture axial loading and deformation. In recent years, Liu et al. [3] have presented a novel pseudo rigid body model that captures the axial deformation and load stiffening, by adding extension springs to capture axial loading, as in Figure 2.3. However, this proposed

model does not capture the stiffness changes that take place around the first buckling mode.

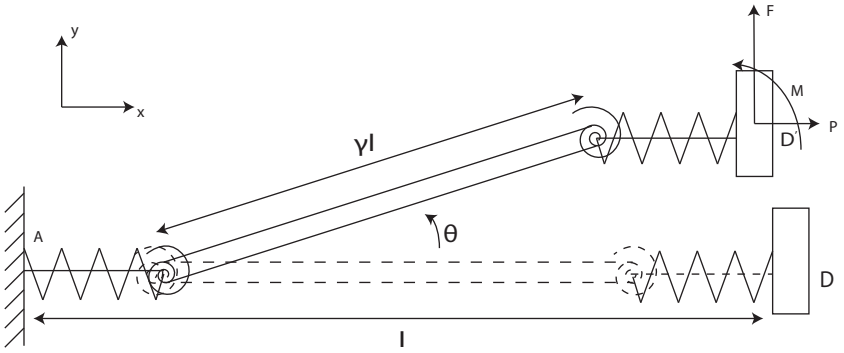

FIGURE 2.3: Fixed-guided beam model with axial loading proposed in [3]

We propose an pseudo rigid body model for fixed-guided beams that is valid for deformations near the buckling region and faithfully captures the stiffness changes around first critical buckling load.

2.3 Impedance Modulation

Variable impedance actuators are mechatronic devices that add physical energy storage and dissipation elements to the actuator such that the impedance of the actuator can be modulated to different levels as necessitated by the interaction. Such actuators are better suited to deal with the contact tasks and interactions with unknown environments, where the performance of stiff actuators fall short. In particular, motion control with high accuracy requires high stiffness levels, while tasks that involves contacts, collisions and shocks require high compliance. Therefore, impedance modulation methods have been proposed to enable modulation to an appropriate impedance level during a task.

Impedance modulation can be achieved by two means, through active control or through introduction of physical energy storage and dissipation elements into the mechanical design. Compliance can be modulated through active control strategies, such as impedance/admittance control. In this approach, the impedance modulation is limited to the control bandwidth of the actuators. Hence, a tool whose impedance is modulated with a controller will behave according to its uncontrolled dynamics under high frequency excitations (impacts) that exceed its control bandwidth. One of the drawbacks of active impedance modulation is that controller may be quite complex and require an accurate dynamic model of the system for high fidelity rendering performance. Moreover, this approach suffers from low energy efficiency, since it requires continuous use of actuators to render the desired impedance. Low energy efficiency becomes a significant limiting factor when untethered and lightweight mobile devices need to be implemented.

As the alternative, impedance modulation can be embedded into the mechanical design. In this approach, the impedance of the tool is adjusted through special mechanisms consisting of passive elastic and dissipation elements, such as springs and dampers. In hardware based impedance modulation, the impedance change is

physical and is valid for the whole frequency spectrum. Mechanical design based impedance modulation requires energy only when the impedance is being modulated; hence, is energy efficient. Furthermore, even though such modulation is commonly performed via actuators to result in variable stiffness actuation, it is possible to utilize this approach without any controllers/actuators by allowing the user to manually adjust the compliance of the tool to match the requirements of the task. In this thesis, stiffness modulation is achieved through exploiting the variable stiffness characteristics of axially loaded buckling beam.

Stiffness is the most commonly modulated part of impedance. Hardware based stiffness modulation can be achieved through three fundamental approaches: i) by loading non-linear compliant elements in an antagonistic arrangement [54–66], ii) by altering the physical properties of a compliant element [67–75], and iii) by adjusting the pre-load of a compliant element [76–89]. Mimicking the antagonist muscle pairs of a human arm, controlling the effective length of a spring, axial loading of a buckling beam, and variable lever arm mechanisms are well-known examples of i) antagonistic control, ii) structural control, and iii) mechanical control approaches, respectively.

Utilizing antagonistic control approach may introduce extra size and complexity to the system. Implementation of nonlinear spring elements are challenging, energy efficiency and energy storage capacity of antagonist arrangement are low. Since antagonistic arrangement is bidirectional with two motors, maximum output power and torque is equal to only one of the motors. On the other hand, antagonistic control approach allows for remote location of actuators which may be advantageous for certain applications.

Physical properties, such as cross section area and/or effective length of the elastic elements can be changed during structural controlled stiffness. This method may be advantageous since it is relatively easy to build and it includes independent stiffness

and equilibrium setting, such that they can be controlled with different motors. On the other hand, it has physical limitations on the range of rendered stiffness levels and energy storage capacity.

Adjusting the pre-load is likely to be the simplest method to implement. Changing the transmission ratio between the output link and spring like element provides better energy efficiency than antagonistic arrangement during stiffness adjustment, since only the adjustment of lever displacement is needed. However, small variation of lever arm may affect stiffness significantly; thus precise position control is required. In addition to the precise position control requirement, friction comes to existence and becomes dominant in small displacements under external loads. Hysteresis effect may also be observed.

Another implementation of mechanical control approach relies on nonlinear buckling characteristics of axially loaded beams. This approach is beneficial since it offers broad range of stiffness changes and inherits the inherent advantages of compliant mechanisms, such as high accuracy and virtually no friction/backlash. Without friction losses this approach can achieve high energy efficiency. Despite these advantages, variable stiffness mechanisms based on axially loaded buckling beams possess limited deflection range which may limit its employment in certain applications.

Chapter 3

Design of the Variable Stiffness Stylus

In this section, we present the design objectives and overview the proposed design solution for the variable stiffness stylus.

3.1 Design Objectives

Various design objectives are considered for the variable stiffness systlus. These objectives are categorized as *imperative*, *optimal*, *primary* and *secondary* objectives according to their priority. This categorization due to Merlet [90] indicates that imperative objectives are the most crucial and must always be met, optimal objectives are related to the performance and needs to be maximized, primary objectives are alterable based on optimal solutions, while secondary objectives are least pressing ones and depends on the preferences of the designer. Table 3.1 includes all criteria taken into consideration during the design of the variable stiffness stylus. Detailed explanation for design objectives is listed below:

TABLE 3.1: Design Objectives

Criteria	**Type**
Adjustable Compliance	Imperative
Scalability	Imperative
Size and Weight	Primary*
Stiffness Range	Primary*
Rendering Fidelity	Primary
Robustness	Primary
Ease of Manufacturing	Secondary
Cost	Secondary

* May be considered as optimal objectives

Adjustable Compliance: The stiffness level of the stylus needs to be adjustable according to requirements of various tasks. Just noticeable difference (JND) indicates the minimum level of stiffness change that can be perceived by humans. According to literature [91], humans can discriminate about 20% stiffness changes from the base value. It is desirable that the stylus can be adjusted to provide at least three different levels of stiffness that are easily noticeable and differentiated by the users. Along these lines, adjustable compliance that ensures at least three different stiffness levels detectable by users is determined as an imperative design criteria.

Scalability: The variable stiffness stylus needs to be implemented in various sizes; hence, scalability without loss of rendering performance (due to friction forces becoming more dominant at micro scales) is considered as an imperative design criteria.

Size and Weight: The variable stiffness stylus should be hand-held, mobile and lightweight for convenient use. These aspects are crucial during the design process and considered as primary objectives. Size and weight can also be considered as optimal objectives, There exists a trade-off between the stiffness range and size. In order to achieve a large stiffness range, optimization techniques may be employed to find optimal size and weight values. In this study, an iterative design approach is taken to determine a large enough stiffness range for a targeted size.

Stiffness Range: The variable stiffness stylus should achieve a large stiffness range, including very compliant levels, without sacrificing the mechanical integrity of the stylus. High stiffness provides more accurate position control, while low stiffness is useful during interacting with soft and fragile objects. As size and weight, stiffness range can be categorized as optimal objective, since an optimization of this criteria is useful.

Rendering Fidelity: Rendering fidelity of the variable stiffness mechanisms are affected by parasitic forces due to friction, backlash, hysteresis avaliable in the system. Rendering fidelity is considered as a primary objective to ensure quality and repeatability of the stiffness rendering performance.

Robustness: The variable stiffness stylus is desired to be robust against manufacturing tolerances, geometric errors, and parasitic motions. Robustness is considered as a primary objective.

Ease of Manufacturing: It is desirable for the manufacturing of the variable stiffness stylus be simple. Complex assemblies and processes should be avoided. Ease of manufacturing is considered as a secondary objective.

Cost: The variable stiffness stylus is expected to be affordable, even as a disposable tool. Along these lines, it should be made of low-cost and easy to manufacture parts. Cost is considered as a secondary objective.

3.2 Proposed Design

We propose a passive (non-actuated) stylus that features manually variable tip stiffness to allow users to adjust tip compliance to match the requirements of various tasks. The stylus consists of a tip, a compliant transmission mechanism, a buckling beam, and a pre-tensioning mechanism, as depicted in Figure 3.1. Stiffness modulation is embedded into the mechanical design through use of a compliant mechanism together with an axially loaded buckling beam. The tip stiffness can be adjusted by controlling the position of a screw that changes the axial loading of the buckling beam. Tensile axial loading of the buckling beam results in significant increase of the transverse stiffness of the beam, while compressive loading can result in negative transverse beam stiffness. Since the stiffness of the stylus tip is governed by the stiffness of the compliant transmission mechanism coupled with the transverse stiffness of the buckling beam, axial loading of the beam can result in a large range of tip stiffness levels.

Featuring a large range of tip stiffness levels though its adjustment mechanism, the

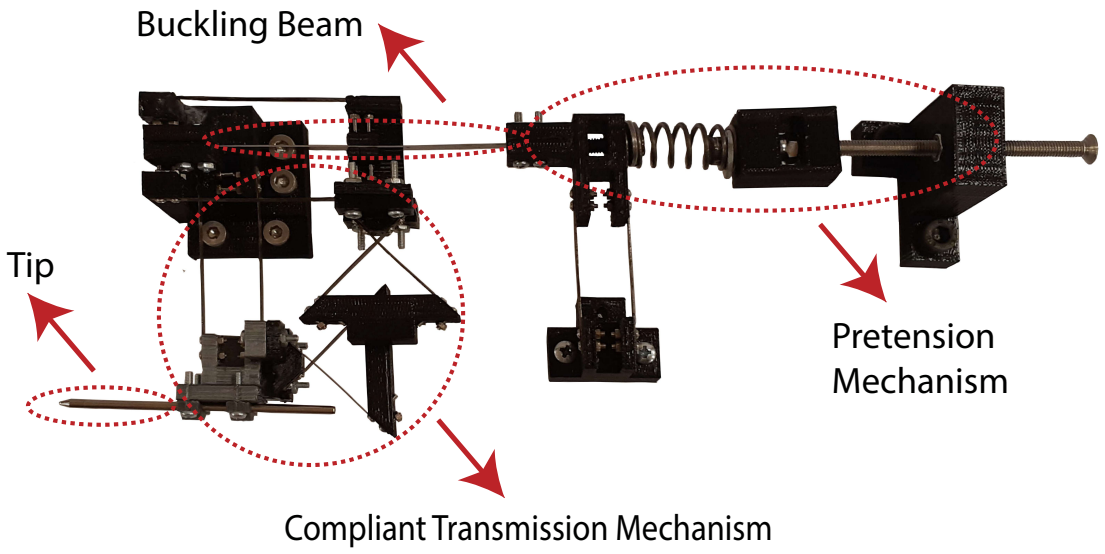

FIGURE 3.1: Variable stiffness stylus

proposed design satisfies the imperative design criteria. In particular, its tip compliance is adjustable and can be tuned such that at least three different perceivable stiffness levels that exceed just noticeable difference thresholds are implemented. Furthermore, thanks to the negative stiffness characteristics of the buckled beam, very low stiffness levels can be achieved without sacrificing the mechanical integrity and load bearing capacity of the stylus.

Furthermore, the proposed solution features a fully compliant design that enables scalability of the variable stiffness stylus to even micro scales. In particular, considering the primary design criteria that aims to minimize size and weight of the device, the long buckling beam is placed along the longitudinal axis of the stylus, parallel to the tip. As a consequence, a power transmission mechanism is necessitated to couple the transverse beam deflections to the tip deflections. A compliant planar parallel mechanism is employed to couple the transverse deflections of the buckling beam to the tip deflections. A planar compliant mechanism is preferred, since such mechanisms are easy to manufacture as monolithic structures at even micro scales and does not display undesired parasitic effects, such as friction and backlash. Consequently, not only the primary objective of size-weight are satisfied, but also the other primary objective of high rendering fidelity is ensured, as the fully compliant design of the stylus minimizes the undesired parasitic forces. Fully compliant design is also necessary to satisfy the imperative design objective of scalability.

A parallel mechanism is preferred for the power transmission, as such mechanisms are known to be more robust against manufacturing errors and dimensional changes due to thermal noise. Furthermore, parallel mechanisms can achieve more precise motion than their serial mechanism counterparts as errors at the joint level are averaged. Moreover, when small deflections are necessitated, parallel mechanisms can be designed to be more compact with higher out-of-plane stiffness. Parallel mechanisms are also advantageous since they allow for grounding of sensors/actuators, if the device needs to be instrumented. Furthermore, beam type flexures are preferred

to implement the compliant mechanisms, since these flexures distribute the stress along the whole body avoiding stress concentrations; hence, has a significantly larger deflection range and life compared to notch type flexures. These design choices help satisfy the secondary design objective of robustness.

Even though the axial loading of the buckling beam can be provided with a position controlled actuator, manual adjustment of tip stiffness is preferred for simplicity and affordability. Currently, it is not clear if continual adjustment of the tip stiffness is necessary to justify such instrumentation. Lack of electronics and actuation mechanism makes the proposed stylus a passive one that requires no batteries. Along with the fully compliant design, these design choices contribute to the secondary objectives of low-cost and ease of manufacturing.

Chapter 4

Modeling and Analysis of the Variable Stiffness Stylus

In this section, we detail the kinematics, stiffness and axial loading analyses of the one degree of freedom stylus with variable tip stiffness. We also derive an equivalent pseudo rigid body model for fixed-guided beams that captures the transverse stiffness change around their first critical buckling load.

4.1 Kinematic Analysis of the Variable Stiffness Stylus

Figure 4.1(a) shows a schematic representation of the variable stiffness stylus where the bold lines denote beam based compliant elements. Axial load is applied through rotation of screw that is attached to a spring. Let θ_1 and θ_2 denote the rotation angles of the cross flexure joints, while s_1 and s_2 represent the displacement of the parallelogram joints. The symbol h is used for the length of lever between the two cross flexure joints. The transverse displacement of the axially loaded beam of

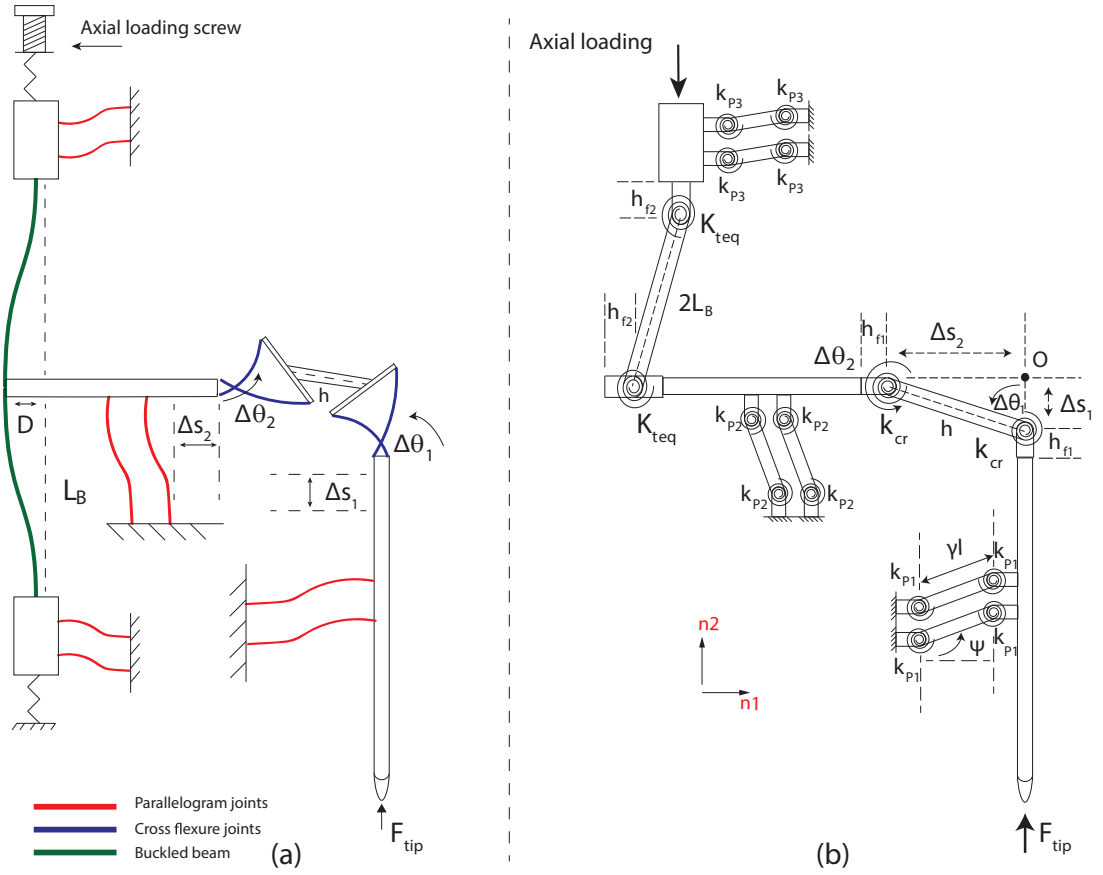

FIGURE 4.1: (a) A schematic representation of the compliant mechanism that enables variable tip stiffness (b) Pseudo-rigid body model of the underlying compliant mechanism

length L_B is represented by D. Kinematic analysis is performed through utilizing the pseudo rigid body model of the system.

Figure 4.1(b) represents an equivalent pseudo rigid body model for Figure 4.1(a). This model involves three basic compliant elements; the parallelogram joints, the cross flexure joints, and the buckling beam, where k_{P1}, k_{P2} , k_{P3} denote the equivalent stiffness values to model the prismatic joints while k_{cr} denotes the torsional stiffness of the cross flexure joints, respectively.

Let N denote the Newtonian reference frame. A parallelogram joint is attached between the screw and the buckling beam, since this parallelogram joint prevents

end points of the buckling beam from rotation and ensure that these end points maintain zero curvature. Pseudo rigid body models of all compliant components of the stylus are presented in Figure 4.1(b).

The kinematics of the pseudo rigid body model is governed by the following relationship:

$$\begin{aligned} s_1\mathbf{n_2} + (\sin\theta_1 h\mathbf{n_1} - \cos\theta_1 h\mathbf{n_2}) - s_2\mathbf{n_1} = 0 \\ (s_1 - h\cos\theta_1)\mathbf{n_2} + (-s_2 + h\sin\theta_1)\mathbf{n_1} = 0 \end{aligned} \tag{4.1}$$

Solving Eqns. 4.1 yields

$$\begin{aligned} s_1 &= h\cos\theta_1 \qquad \Delta s_1 = -h\sin\theta_1\Delta\theta_1 \\ s_2 &= h\sin\theta_1 \qquad \Delta s_2 = h\cos\theta_1\Delta\theta_1 \\ \theta_2 &= 270 + \theta_1 \qquad \Delta\theta_1 = \Delta\theta_2 \end{aligned} \tag{4.2}$$

where Δs_1 and Δs_2 represent the linear displacement along n_2 and n_1 unit directions, respectively. Symbols $\Delta\theta_1$ and $\Delta\theta_2$ are the angular displacement of the cross flexure joints. θ_1 and θ_2 are measured with respect to n_2 and n_1 axes respectively and counterclockwise displacements are considered as positive. All variables can be written with respect to the tip displacement Δs_1 as follows, in order to facilitate the further analysis:

$$\Delta\theta_1 = -\frac{\Delta s_1}{h\sin\theta_1} \qquad \Delta\theta_2 = -\frac{\Delta s_1}{h\sin\theta_1} \qquad \Delta s_2 = -\frac{\Delta s_1}{\tan\theta_1} \tag{4.3}$$

4.2 Stiffness Analysis of the Variable Stiffness Stylus

The overall stiffness of the variable stiffness stylus is analyzed by first studying the pseudo rigid body model of each compliant element and then invoking virtual work principle. Following sections present these analyses.

4.2.1 Compliant Parallelogram Joint

Pseudo rigid body model of a parallelogram joint is constructed with two equivalent parallel beams, as shown in Figure 4.2. For small deflections, a parallelogram joint has similar behaviour as a prismatic joint and allows motion on only one translational axis. Note that $\Delta\theta_p$ is the angle between n_1 axis and deflected beams, l_p is the length of links made of compliant beams, γl_p denotes the effective length between two torsional springs, F_p is the force applied along the n_1 axis, and Δx_p is the linear displacement of parallelogram within the n_1 axis.

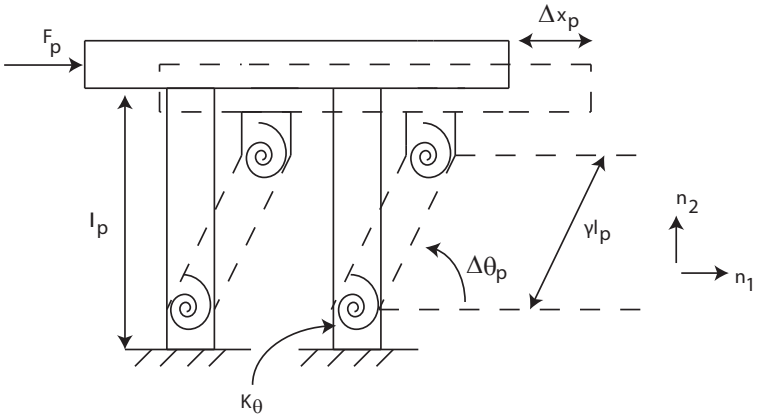

FIGURE 4.2: Pseudo rigid body model of a parallelogram joint

To find equivalent pseudo rigid body model, the fixed-guided beam model proposed in [1] is utilized. One end of the beams are cantilevered while other ends are moving

without changing their angle with respect to the n_1 axis. As stated in [1], the equivalent torsional stiffness for the fixed-guided beam model can be derived as

$$K_\theta = 2\gamma K_f(EI/l_p) \tag{4.4}$$

where K_θ is the torsional spring constant, E is the elastic modulus of the beam, and I is the area moment of inertia. The coefficient γ is taken as 0.8517, while K_f is 2.67617. Also, the maximum deflection for fixed guided beam is estimated as 64.3°. Elaborative analysis and derivation of these parameters can be found in [1].

In order to calculate the stiffness of the parallelogram joint along the n_1 axis, the virtual work principle can be used as follows to result in

$$x_p = \gamma\, l_p\, \sin\theta_p$$

$$\text{invoke small angle approximation as } \sin\theta_p \approx \theta_p$$

$$x_p = \gamma\, l_p\, \theta_p$$

$$K_p\, \Delta x_p\, \delta x_p = 4\, K_\theta\, \Delta\theta_p\, \delta\theta_p$$

$$K_p\, \gamma\, l_p\, \Delta\theta_p\, \gamma\, l_p\, \delta\theta_p = 4\, K_\theta\, \Delta\theta_p\, \delta\theta_p$$

$$K_p = \frac{8\, K_\theta\, E\, I}{\gamma\, l_p^3} \tag{4.5}$$

4.2.2 Cross Flexure Joint

A compliant cross flexure joint behaves similar to a revolute joint, allowing almost pure rotational motion for a range of deflections. To model the cross flexure joint, we use the pseudo rigid body model presented in [92], which proposes a simple equivalent pin joint model as shown in Figure 4.3.

According to this model the equivalent stiffness of the cross flexure joint is given as

$$k_{cr} = \frac{8\,E\,I\,(1 - 3n + 3n^3)n\,\cos\psi}{h_m} \tag{4.6}$$

where h_m is the horizontal distance between the pivot point O and moving frame D. The coefficient n is determined based on the proportion of h to the distance between moving frame D and fixed frame E.

Moreover, the maximum deflection ϕ_{max} can be estimated as

$$\phi_{max} = \frac{h_m\,S_y}{E\,t\,(3n - 1)n\,\cos\beta} \tag{4.7}$$

where S_y represents the yield strength, while t denotes the thickness of the beam.

In our design, ψ is taken as 45°, while n is chosen as 0.873 as these value have been shown to minimize the centre shift.

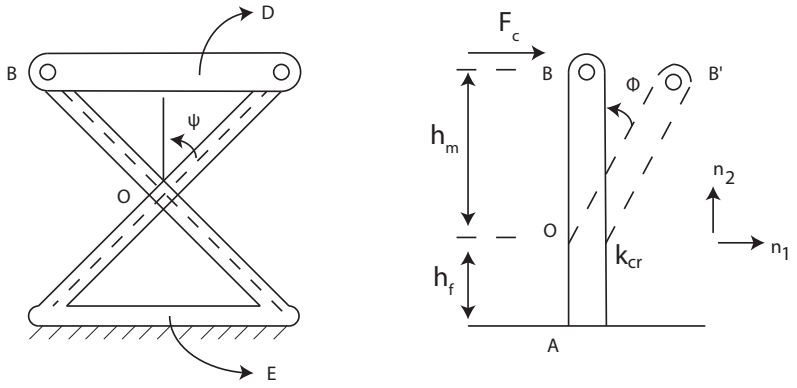

FIGURE 4.3: Pseudo rigid body model of cross flexure joint

4.2.3 Buckling Beam

Negative stiffness characteristic of the buckling beam is significant to ensure desired variable stiffness feature. Figure 4.4 presents a schematic representation of a buckling beam under compressive forces, where D denotes transverse deflection, $2R$ represents transverse loading, L_b is the half length of beam, and L stands for the full length of the beam.

Axially loaded beams possess dominant linear and cubic spring constants around their buckling loads. In particular, the linear stiffness coefficient is related to displacement of system along the n_1 axis, while the cubic stiffness coefficient is related to the third power of the same displacement. Together, they dominate the transverse stiffness of the buckling beam and provide adjustable stiffness characteristics for the variable stiffness actuator design in [86].

Let F_a be the axial load on the buckling beam, P_{cr} be the first critical buckling load, K be the equivalent actuator stiffness and μ be the dimensionless variable that captures the ratio between the actuator stiffness and the axial stiffness of the beam. The linear k_l and the cubic stiffness k_c coefficients are given in [93]

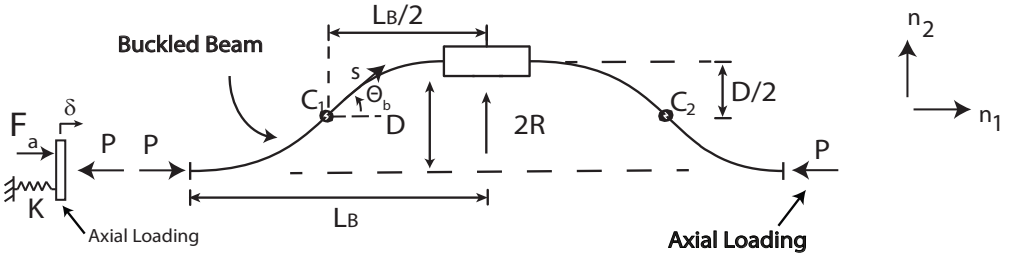

FIGURE 4.4: Schematic representation of a buckling beam

$$k_l = -\frac{P_{cr}}{2L}\frac{(F_a - P_{cr} - P_{cr}\mu)\pi^2}{P_{cr}(1+\mu)} \tag{4.8}$$

$$k_c = \frac{P_{cr}}{8L^3}\left(\frac{AE\mu}{P_{cr}(1+\mu)} - \frac{4}{3}(\frac{F_a}{P_{cr}(1+\mu)} - 1)\right)\pi^4 \tag{4.9}$$

Equations 4.8 and 4.9 are derived from the Euler-beam equations around the first critical buckling load and under small deflection assumption. If the compressive force exceeds the first critical buckling load of the beam, negative stiffness along the transverse direction has been acquired. Negative stiffness characteristic is valid under the assumption that deflection is kept small. When deflection gets large, the cubic term dominates and significantly affecting the overall the stiffness. Moreover, the transverse stiffness value can be increased by applying tensile forcing to the beam.

In order to decrease the complexity of the analysis, simplify integration with the

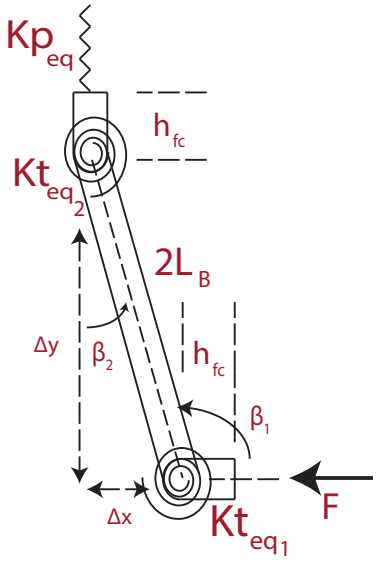

FIGURE 4.5: Equivalent pseudo rigid body model of a buckling beam that captures stiffness change around the critical buckling load

existing pseudo rigid body models of other compliant joints, this continuum model of buckling beam is replaced with an equivalent pseudo rigid body model. This lumped parameter model provided by pseudo rigid body modeling promote ease of design by hiding the underlying modeling complexities of continuum mechanics from the designer.

Figure 4.5 presents the proposed equivalent pseudo rigid body model of the buckling beam that captures the stiffness changes around the first critical buckling load. This pseudo rigid body model is derived by applying virtual work principle and ensuring equivalence with the analytical model given in Eqns. 4.8 and 4.9.

The equivalent pseudo rigid body model features two torsional springs and a linear spring that captures the axial load dependent properties of buckling beams. The equivalent torsional spring constant $K_{t_{eq}}$ and linear spring constant $K_{p_{eq}}$ are derived as

$$K_{t_{eq}} = \frac{L^2}{2}\, k_l \tag{4.10}$$

$$K_{p_{eq}} = L^2\, k_c - \frac{2}{3}\, k_l \tag{4.11}$$

Details of stiffness and pseudo rigid body modeling of buckling beams around their critical buckling loads is presented in Section 5.2.

4.2.4 Tensioning Mechanism

Figure 4.6 (a) depicts a lumped parameter model of the pre-tensioning mechanism that is used to axially load the buckling beam. Note that parallelogram joints with stiffness K_p are utilized to ensure that the end points of the buckling beam are guided, that are rotation free, always maintaining zero curvature. Consequently, the effect of these compliant mechanisms are also considered while calculating the equivalent stiffness of the tensioning mechanism. Axial forcing is exerted by applying an appropriate amount of deflection to the pre-tensioning spring K_s.

Figure 4.6 (b) presents an equivalent force controlled actuation model for axially loading the beam. Here, K stands for the actuator stiffness, while F_a represents the actuator force.

Equating both sides of Figure 4.6 to each other, the equivalent actuator force and stiffness of the pre-tension mechanism can be derived as

$$F_a = K_s \Delta_p \tag{4.12}$$

$$K = K_p + K_s \tag{4.13}$$

where Δ_p represents the axial displacement of the adjustable end of the pre-tension spring.

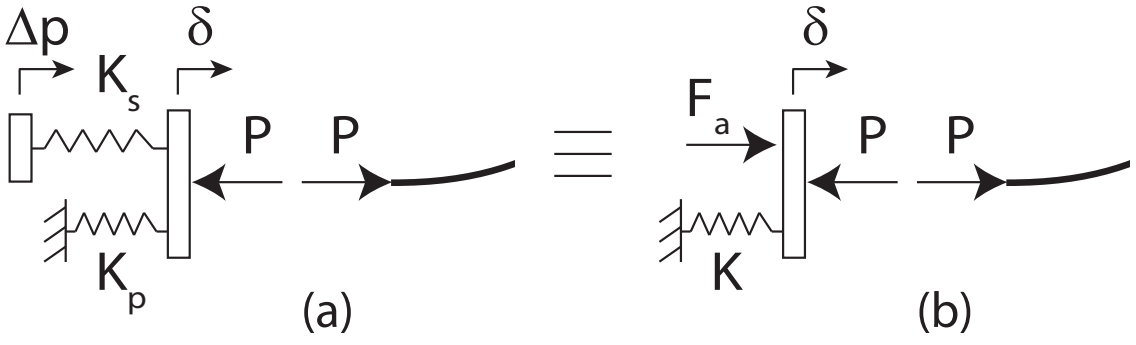

FIGURE 4.6: Lumped parameter model of the tensioning mechanism

Once the equivalent stiffness of the tensioning mechanism is determined, desired axial forcing can be applied to the buckling beam by imposing relevant deflection to the tensioning mechanism. In other words, through a good estimate of the equivalent stiffness of the tensioning mechanism, the force control problem problem can be converted into a position control problem, in the spirit of series elastic actuation. Given precise motion control is significantly easier and more robust than force control, existence of tensioning springs to control the axial loading is an important feature of the design.

4.2.5 Tip Stiffness of the Variable Stiffness Stylus

Virtual work principle is used to determine the overall stiffness of the variable stiffness stylus when the tip moves along the n_2 axis. According to the virtual work principle, a system is in equilibrium under the action of forces if the total virtual work done by these forces is zero for any admissible virtual displacement of the system. In our case, the forces due to the compliant elements are considered. Linear stiffness values of parallelogram joints are denoted as K_{p1} and K_{p2}, while the torsional stiffness of the cross flexure joints are denoted as k_{cr}.

Referring to Figure 4.1(b), the force-deflection relationship is governed through the following equations

$$\delta s_1 = -h\ \sin\theta_1\ \delta\theta_1$$

$$\delta s_2 = h\ \cos\theta_1\ \delta\theta_1$$

$$F_{tip}\ \delta s_1 = K_{p1}\ \Delta s_1 \delta s_1 + k_{cr}\ \Delta\theta_1\ \delta\theta_1 + k_{cr}\ \Delta\theta_2\ \delta\theta_2 + K_{p2}\ \Delta s_2\ \delta s_2 + k_l\ \Delta s_2\ \delta s_2 + k_c\ (\Delta s_2)^3\ \delta s_2$$

$$F_{tip}\ \delta s_1 = K_{p1}\ \Delta s_1\ \delta s_1 + k_{cr}\ \frac{\Delta s_1}{-h\sin\theta_1}\ \frac{\delta s_1}{-h\sin\theta_1} + k_{cr}\ \frac{\Delta s_1}{-h\sin\theta_1}\ \frac{\delta s_1}{-h\sin\theta_1} + K_{p2}\ \frac{-\Delta s_1}{\tan\theta_1}\ \frac{-\delta s_1}{\tan\theta_1}$$
$$+k_l\ \frac{-\Delta s_1}{\tan\theta_1}\ \frac{-\delta s_1}{\tan\theta_1} + k_c\ (h\cos\theta_1\ \Delta\theta_1)^3\ (h\cos\theta_1\ \delta\theta_1)$$

$$F_{tip}\ \delta s_1 = \left[K_{p1} + \frac{k_{cr}+k_{cr}}{h^2\sin^2\theta_1} + (K_{p2}+k_l)\cot^2\theta_1\right]\ \Delta s_1\ \delta s_1 + k_c\ h^4\ \cos^4\theta_1\ (\Delta\theta_1)^3\ \delta\theta_1$$

$$F_{tip}\ \delta s_1 = \left[K_{p1} + \frac{k_{cr}+k_{cr}}{h^2\sin^2\theta_1} + (K_{p2}+k_l)\cot^2\theta_1\right]\ \Delta s_1\ \delta s_1 + k_c\ h^4\ \cos^4\theta_1\ (\frac{\Delta s_1}{-h\sin\theta_1})^3 \frac{-\delta s_1}{-h\sin\theta_1}$$

$$F_{tip} = \left[K_{p1} + \frac{k_{cr}+k_{cr}}{h^2\sin^2\theta_1} + (K_{p2}+k_l)\cot^2\theta_1\right]\ \Delta s_1 + k_c\ (\cot^4\theta_1)\ (\Delta s_1)^3 \tag{4.14}$$

Given that the total stiffness can be separated into linear K_{lin} and cubic K_{cub} terms, the equivalent stiffness of the variable stylus tip can be determined as follows:

$$F_{tip} = K_{lin}\,\Delta s_1 + K_{cub}\,(\Delta s_1)^3 \implies$$

$$K_{lin} = \left[K_{p1} + (K_{p2} + \frac{2K_{t_{eq}}}{L^2})(\cot^2\theta_1)\right] + \left[\frac{2k_{cr}}{(h\sin\theta_1)^2}\right] \tag{4.15}$$

$$K_{cub} = \frac{K_{p_{eq}}}{L^2} + \frac{4K_{t_{eq}}}{3L^4}\,\cot^4\theta_1 \tag{4.16}$$

Note that k_l and k_c is replaced with $\frac{2K_{t_{eq}}}{L^2}$ and $\frac{K_{peq}}{L^2} + \frac{4K_{t_{eq}}}{3L^4}$ respectively.

4.2.6 Discussion

The equivalent pseudo rigid body model for the buckling beam and the pseudo rigid body model of the compliant transmission mechanism possess some similarities. Figure 4.7 presents the similarities between the compliant transmission mechanism and the equivalent pseudo rigid body model for the buckling beam. In order to achieve equivalent models, the Newtonian reference frame needs to be rotated by $\pi/2$ counterclockwise, and then reflected with respect to the vertical plane.

In particular, if K_{p1} and k_l are taken as zero, $\theta_1 + 3\pi/4$ is taken as θ_2 and k_{cr} is equal to both k_{cr1} and k_{cr2}, then Eqn. 4.15 becomes

$$K_{lin} = \left[(K_{p2})(\tan^2\theta_2)\right] + \left[\frac{2k_{cr}}{(h\cos\theta_2)^2}\right] \tag{4.17}$$

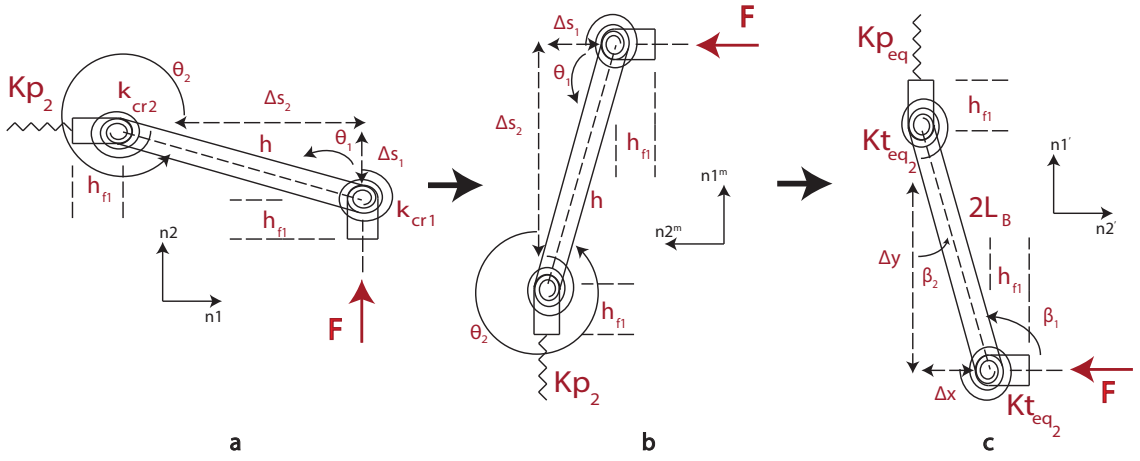

FIGURE 4.7: Relation between the pseudo rigid body model of the compliant transmission mechanism and the proposed equivalent pseudo rigid body model for the buckling beam. (a) presents the compliant transmission mechanism in the stylus, (b) presents this model after $\pi/2$ counterclockwise rotation, and (c) depicts the equivalent pseudo rigid body model for the buckling beam.

Calculating the Taylor series expansion of Eqn. 4.17 with respect to s_1 around zero and keeping first order terms yields

$$F = \left[\frac{2k_{cr}}{h^2}\right]\Delta s_1 + \left[\frac{K_{p2}}{h^2} + \frac{4k_{cr}}{3h^4}\right](\Delta s_1)^3 \tag{4.18}$$

which derives the same result as the equivalent pseudo rigid body model given in Eqn. 5.26.

Chapter 5

Pseudo Rigid Body Model of the Buckling Beam

This chapter presents the analytical beam model under axial loading near its first critical buckling load, derives an equivalent proposed pseudo rigid body model of the buckling beam, experimentally verifies the model and justifies the need for such a novel pseudo rigid body model to properly capture the stiffness changes.

5.1 Analytical Model of the Buckling Beam

This section lists the underlying assumptions and presents the detailed analytical derivation the continuum beam model as in [93].

The derivation closely follows [93] and is performed under the following assumptions:

- Only the first buckling mode contributes to the transverse deformation of the beam.
- The transverse deformation of the beam is governed by a cosine shape.

- The relationship between the axial displacement of beam x_a and the transverse deformation of middle of the beam x_t is given as:

$$x_t = \sqrt{\frac{4Lx_a}{\pi^2}} \tag{5.1}$$

  where L represents the full length of the beam.

- All materials' behaviour is linear elastic. All strains are small, while x_t can be large, as long as $x_t/L << 1$.

- Axial elastic deformation of the beam due to the applied compressive force is much less than full length of the beam.

- The slope of the deformed beam is small compared to unity.

As illustrated in Figure 5.1, s is the variable that is used to measure the path length along the deflected beam. θ_b is the angle between the tangent of beam at s and the horizontal direction. Let

$$x = \int_0^s \sqrt{1-(y')^2}ds \tag{5.2}$$

where $x(s)$ is the horizontal projection of s. From the moment curvature relation

$$\frac{M}{EI} = \frac{-Py - Rx}{EI} = \frac{d\Theta_b}{ds} = \frac{y''}{\sqrt{1-(y')^2}} \tag{5.3}$$

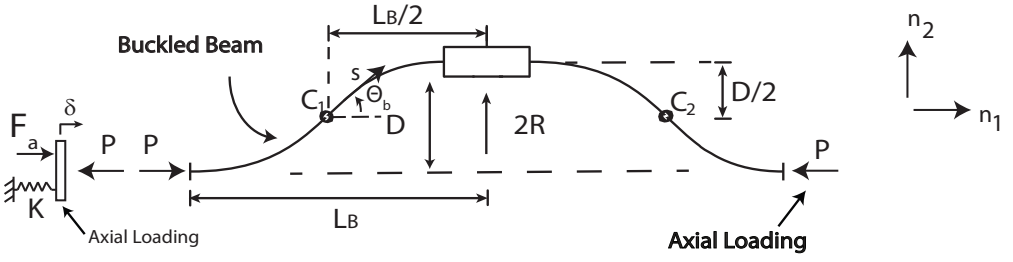

FIGURE 5.1: Schematic representation of a buckling beam

where $y(0) = 0$ and $y(L/4) = D/2$ are the boundary conditions. When $|y'| << 1$, $\frac{M}{EI}$ can be approximated as

$$\frac{-Py - R\int_0^s \sqrt{(1\frac{-(y')^2}{2}}}{EI} ds = y''(1 + \frac{(y')^2}{2}) \tag{5.4}$$

and higher terms ($(y')^4$ and higher) are neglected. We can define

$$y = \frac{D \sin ws}{2} \quad w = \frac{2\pi}{L} \tag{5.5}$$

Arranging Eqn. 5.4 with Eqn. 5.5 yields

$$\begin{aligned} \frac{-PD\sin(ws)}{2} - Rs + \frac{R\pi^2 D^2}{4L^2} + \frac{R\pi D \sin(2ws)}{8L} \\ + \frac{EIDw^2 \sin(ws)}{2} + \frac{EID^3 w^4 \sin(ws)\cos^2(ws)}{16} - R(D,s) = 0 \end{aligned} \tag{5.6}$$

where $R(D, s)$ is defined as residual error. By applying Galerkin's method

$$\int_0^{L/4} \sin(ws) R(D,s) ds = 0 \tag{5.7}$$

one can derive the following explicit equation:

$$\frac{PD_1}{P_{cr}L} + \frac{2R}{P_{cr}\pi^2} - \frac{8R(D_1)^2}{3P_{cr}L^2} = \frac{D_1}{L} + \frac{(D_1)^3\pi^2}{2L^3} \tag{5.8}$$

One can simplify Eqn. 5.8 with respect to D_1 to obtain

$$\frac{P}{P_{cr}}\left(\frac{D_1}{L}\right) + \frac{R}{P_{cr}}\left[\frac{2}{\pi^2} - \frac{8}{3}\left(\frac{D_1}{L}\right)^2\right] = \frac{D_1}{L}\left[1 + \frac{\pi^2}{2}\left(\frac{D_1}{L}\right)^2\right] \tag{5.9}$$

where $\frac{P_{cr}}{L}$ and $\frac{D_1}{L}$ are the normalized first critical load of the buckling beam and transverse deflection, respectively, and $\frac{D}{2} = D_1$.

The net axial load P on the beam can be expressed as

$$P = F_a - K(\delta) \tag{5.10}$$

where δ equals to $x_a + x_t$ and $K(x_a + x_t)$ is the restoring force of the actuator, with K denoting the actuator stiffness.

Note that restoring force against elastic deformation becomes $K_{axial}(x_a)$ axial load applied to deflecting beam spring can be obtained as

$$P = (F_a - Kx_t)\left[\frac{K_{axial}}{K + K_{axial}}\right] \tag{5.11}$$

where K_{axial} is the axial stiffness of the beam and equals to EA/L. Here, E and A are defined as the elastic modulus of the beam and the cross section area of the beam, respectively.

We here define non-dimensional variables $\xi = D_1/L$ and $\mu = K/K_{axial}$ under the small deflection assumption $\xi << 1$. One can obtain the below results by solving Eqns. 5.11 and 5.9 together and applying Taylor expansion with respect to transverse displacement D around zero:

$$\frac{2R}{P_{cr}} = -K_{ln}\xi + K_{cn}\xi^3 \tag{5.12}$$

$$K_{ln} = \left(\frac{F_a}{P_{cr}(1+\mu)} - 1\right)\pi^2 \tag{5.13}$$

$$K_{cb} = \left(\frac{AE\mu}{P_{cr}(1+\mu)} - \frac{4}{3}\frac{F_a}{P_{cr}(1+\mu)} - 1\right)\pi^4 \tag{5.14}$$

where K_{ln} and K_{cb} are the non-dimensional linear and cubic spring constants.

Dimensional linear k_l and cubic k_c stiffness values can be determined as

$$k_l = \frac{P_{cr}}{2L}\left(\frac{F_a}{P_{cr}(1+\mu)} - 1\right)\pi^2 \tag{5.15}$$

$$k_c = \frac{P_{cr}}{8L^3}\left(\frac{AE\mu}{P_{cr}(1+\mu)} - \frac{4}{3}\frac{F_a}{P_{cr}(1+\mu)} - 1\right)\pi^4 \tag{5.16}$$

5.2 Equivalent Pseudo Rigid Body Model of the Buckling Beam

In this section, we derive an equivalent pseudo rigid body model for fixed-guided beams that captures their stiffness change around their first critical buckling load.

Given the pseudo rigid body model of buckling beam as depicted in Figure 5.2, the virtual work principle is utilized to calculate the linear and cubic stiffness coefficients for the model. In particular, the stiffness of the pseudo rigid body model is equated to the stiffness from the analytical solution found in Section 5.1 to form two equations with two unknowns, through which equivalent torsional and linear spring coefficients are derived. Let

$$x = L \sin\beta_2 \quad and \quad y = L \cos\beta_2 \tag{5.17}$$

where x denotes the transverse position, y represents the axial position, and β_2 is the rotation angle of the torsional spring $K_{t_{eq2}}$ according to kinematics of the model.

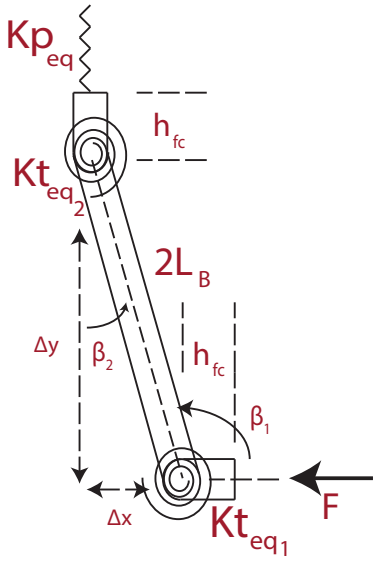

FIGURE 5.2: Equivalent pseudo rigid body model of a buckling beam that captures stiffness change around the critical buckling load

Accordingly, the displacements are related as

$$\Delta x = L\ \cos\beta_2\ \Delta\beta_2 \quad and \quad \Delta y = -L\ \sin\beta_2\ \Delta\beta_2 \tag{5.18}$$

Please note that $\beta_2 + \pi/2 = \beta_1$, $\Delta\beta_1 = \Delta\beta_2$ and $K_{t_{eq1}} = K_{t_{eq2}} = K_{t_{eq}}$. The virtual work principle is applied as follows

$$F\ \delta x = K_{t_{eq1}}\ \Delta\beta_1\ \delta\beta_1 + Kt_{eq_2}\ \Delta\beta_2\ \delta\beta_2 + K_{p_{eq}}\ \Delta y\ \delta y \tag{5.19}$$

$$F\ \delta x = K_{t_{eq}}\ \frac{\Delta x}{L\cos\beta_2}\ \frac{\delta x}{L\cos\beta_2} + K_{t_{eq}}\ \frac{\Delta x}{L\cos\beta_2{}'}\ \frac{\delta x}{L\cos\beta_2} + K_p\ \frac{-\Delta x}{\cot\beta_2}\ \frac{-\delta x}{\cot\beta_2} \tag{5.20}$$

Next, small angle approximation is used and Taylor series expansion is taken around $\beta_2 = 0 + \Delta\beta_2$ and $x = 0 + \Delta x$. Rearranging Eqn. 5.20 yields to

$$F = \left[\frac{K_{t_{eq}}}{(L\cos\beta_2)^2} + \frac{K_{t_{eq}}}{(L\cos\beta_2)^2}\right]\Delta x + \frac{K_{p_{eq}}}{\cot^2\theta_2{}'}\Delta x \tag{5.21}$$

$$F = \left[\frac{2K_{t_{eq}}}{(L\cos\beta_2)^2} + \frac{K_{p_{eq}}}{\cot^2\beta_2}\right]\Delta x \tag{5.22}$$

Next substitute in $y = L\ \cos\beta_2$ and $y = \frac{x}{-\tan\beta_2}$ such that

$$F = \left[\frac{2K_{t_{eq}}}{(y)^2} + \frac{K_{p_{eq}}}{\cot^2\beta_2}\right]\Delta x \tag{5.23}$$

$$F = \left[\frac{2K_{t_{eq}}}{(\frac{x}{-\tan\beta_2})^2} + \frac{K_{p_{eq}}}{\cot^2\beta_2}\right]\Delta x \tag{5.24}$$

$$\frac{F}{\Delta x} = \left[\frac{2K_{t_{eq}}(-\tan\beta_2)^2}{x^2} + \frac{K_{p_{eq}}}{(\cot\beta_2)^2}\right] \tag{5.25}$$

After taking Taylor series expansion of Eqn. 5.25, where β_2 is defined as $\frac{x}{L}$, the result reads as

$$F = \left[\frac{2K_{t_{eq}}}{L^2}\right]\Delta x + \left[\frac{K_{p_{eq}}}{L^2} + \frac{4K_{t_{eq}}}{3L^4}\right](\Delta x)^3 \tag{5.26}$$

The equivalent torsional and linear spring coefficients in pseudo rigid body model can be derived by equating Eqn. 5.26 to 4.8 and 4.9 as follows:

$$K_l = \frac{2K_{t_{eq}}}{L^2} \tag{5.27}$$

$$K_c = \frac{K_{p_{eq}}}{L^2} + \frac{4K_{t_{eq}}}{3L^4} \tag{5.28}$$

These two equations can be solved for two unknowns of $K_{t_{eq}}$ and $K_{p_{eq}}$ as follows. Using Eqn. 5.27, the equivalent torsional spring coefficient $K_{t_{eq}}$ can be expressed as

$$K_{t_{eq}} = \frac{K_l\, L^2}{2} \tag{5.29}$$

Similarly, the linear stiffness coefficient $K_{p_{eq}}$ can be calculated by substituting $K_{t_{eq}}$ with $\frac{K_l\, L^2}{2}$ in Eqn. 5.28 to lead to

$$K_c = \frac{K_{p_{eq}}}{L^2} + \frac{4}{3L^4}\frac{K_l\, L^2}{2} \tag{5.30}$$

$$3L^4 K_c = 3L^2 K_{p_{eq}} + 2L^2 K_l \tag{5.31}$$

$$3L^4 K_c - 2L^2 K_l = 3L^2 K_{p_{eq}} \tag{5.32}$$

$$K_{p_{eq}} = K_c\, L^2 - \frac{2K_l}{3} \tag{5.33}$$

5.3 Experimental Verification

This section presents experimental verification of the equivalent pseudo rigid body model for the buckling beam that captures the stiffness changes. Three different beams under different axial load conditions have been equal to the same pseudo rigid body model which consist of two cross flexure joints and a parallelogram joint.

5.3.1 Experimental Setup

Experimental setup used for the verification of the proposed equivalent pseudo rigid body model is shown in Figure 5.3. This setup consists of an optical encoder (US Digital EM1 with 2000 counts/inch resolution under quadrature decoding), a force sensor (ATI Nano 25) with 1/16 N resolution attached to a linear slider to apply to the tip and measure the applied force and a PC based I/O interface (Quanser Q8-USB) for real-time data acquisition. In order to acquire stiffness estimates of the variable stiffness stylus, the beam is repeatedly pressed with the force sensor and transverse displacement versus applied force data are collected. The stiffness is estimated through the slope of a best line fit to this data.

The mechanical implementation consists of three different buckling beams cut to match three different first critical buckling loads, two compliant prismatic joints used to guide beam ends and prevent inflection points of buckling beam from undesired rotations, and two 3D printed adjustment parts between the pre-tensioning spring and the screw. Table 5.1 lists the relevant dimensions and physical properties of the beams used for the verification of the proposed equivalent pseudo rigid body model.

TABLE 5.1: Propertied of the Buckling Beams

Parallelogram joint beam height[mm]	5
Parallelogram joint beam width[mm]	0.6
Parallelogram joint beam full length - effective length[mm]	60 - 29
Buckling beam (Applied load=0) height[mm]	17.9646
Buckling beam (Applied load=0) width[mm]	0.6
Buckling beam (Applied load=0) full length - effective length[mm]	340 - 288.2094
Buckling beam (Applied load=0.3Pcr) height[mm]	25.8736
Buckling beam (Applied load=0.3Pcr) width[mm]	0.6
Buckling beam (Applied load=0.3Pcr) full length - effective length[mm]	340 - 288.2352
Buckling beam (Applied load=0.6Pcr) height[mm]	45.6512
Buckling beam (Applied load=0.6Pcr) width[mm]	0.6
Buckling beam (Applied load=0.6Pcr) full length - effective length[mm]	340 - 288.2606

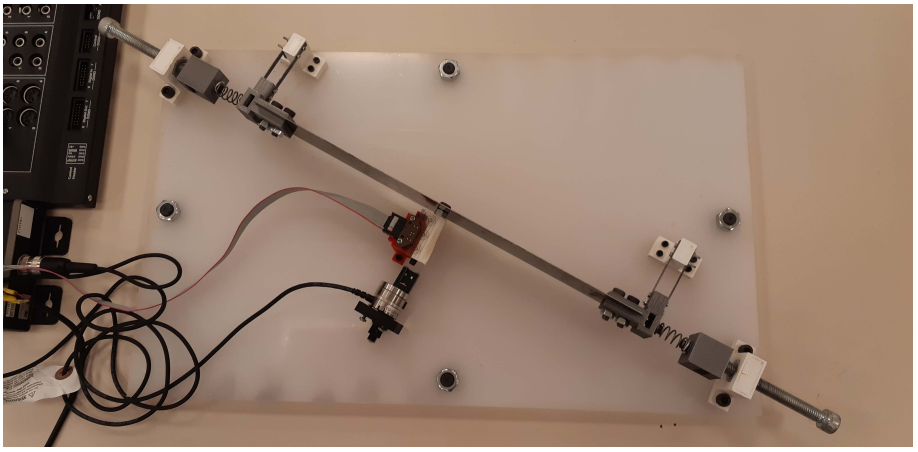

FIGURE 5.3: Experimental setup used for the characterization of the proposed equivalent pseudo rigid body model

5.3.2 Verification Results

Proposed equivalent pseudo rigid body model has been verified under three different load conditions: no axial force, $0.3P_{critical}$, and $0.6P_{critical}$. Figures 5.4–5.6 depict the characterization results from these experiments with least squares linear fits on the data. Experimental characterization of the proposed model is performed through applying a force to the screw at the middle of the beams by pressing the force sensor that is rigidly attached to linear slider. During measuring the force, displacement of the middle of the beam is recorded by encoder. After saving both values, force vs. displacement graph is plotted and least square linear fit is implemented. This procedure is applied at least ten times to obtain experimental data correctly. Both results at these three different load conditions fit well with the experimental data as depicted in below figures.

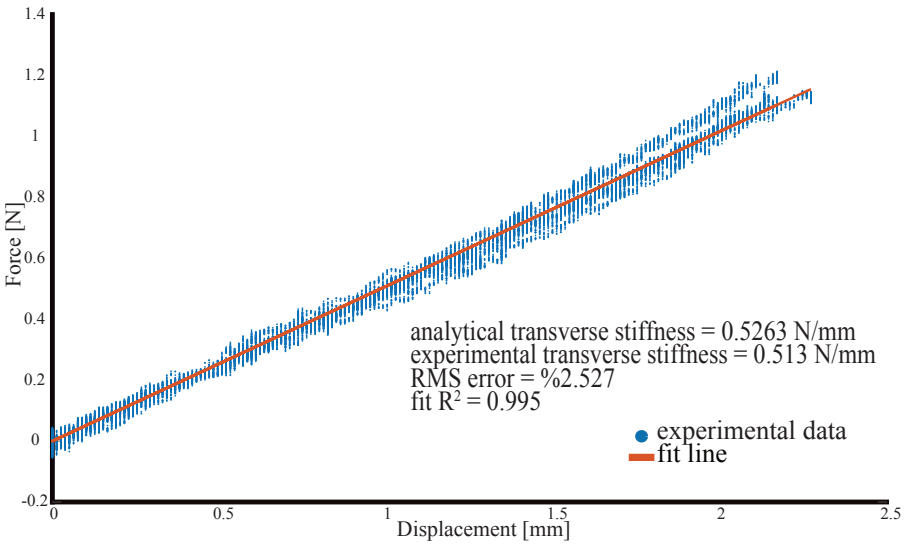

FIGURE 5.4: Equivalent pseudo rigid body model at 0 load

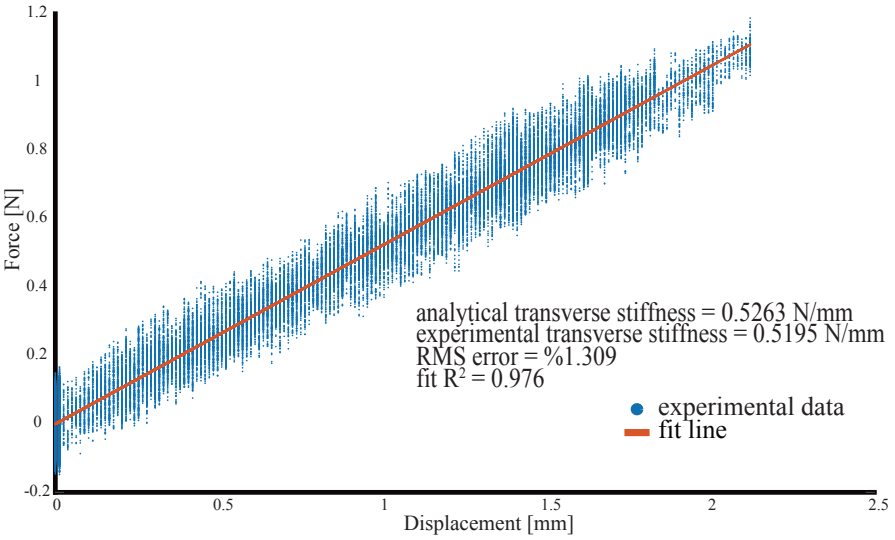

FIGURE 5.5: Equivalent pseudo rigid body model at 0.3 Pcr load

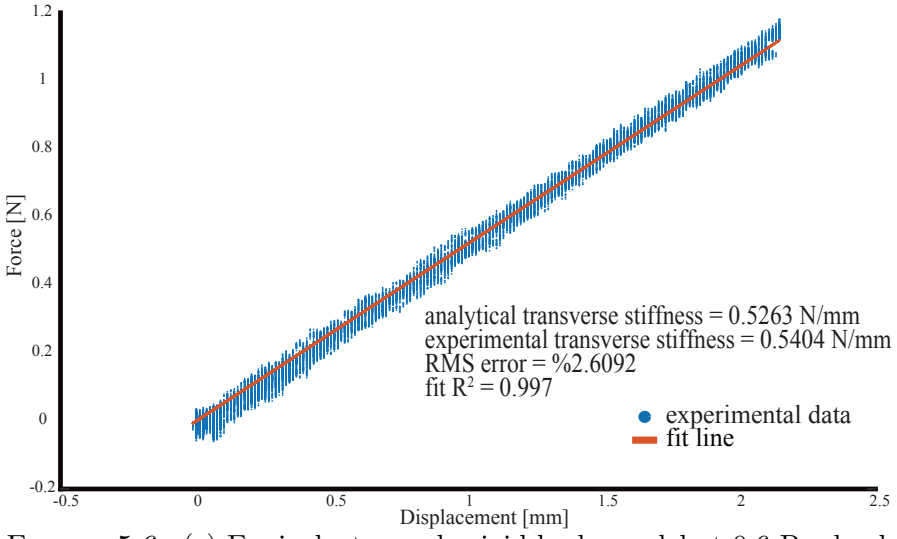

FIGURE 5.6: (c) Equivalent pseudo rigid body model at 0.6 Pcr load

5.3.3 Discussion

The proposed equivalent pseudo rigid body model is experimentally verified. It is shown that there exists a good agreement between analytical and experimental transverse stiffness values. For all three cases, error is less than 2.7%. Stiffness characterization differences between these three cases can be possible due to the challenges in the implementation of perfect boundary conditions, possible misalignments in the direction of the applied force on the tip, the manufacturing tolerances that affect geometric parameters of the spring steel sheets and errors caused due to assembly.

In the literature, several pseudo rigid body models for fixed-guided beams have been proposed [1, 2, 53]; however, none of these models focus on the bending deformations and these models fail to capture the axial loading and deformation characteristics of the beams, with the exception of the model proposed by Liu et al. [3].

The model proposed in [3] is incapable of capturing the stiffness changes under axial loading. Figure 5.7 presents the comparison of the model in [3] and proposed pseudo rigid body model for fixed guided beams. Note that proposed model is based on the analytical solution of buckling beams proposed in [93]. In particular, Figure 5.7 is plotted for the aluminum alloy (AI7075-T6) beams with elastic modulus, length, thickness and height taken as 71 GPa, 30 mm, 0.5 mm and 10 mm, respectively.

Both model exhibits similar behaviour for small displacements except than the compressive force which is greater than first critical buckling load of the beam. Figure 5.7 clearly indicates that the model proposed by Liu et al. [3] does not capture the stiffness changes under different axial loading conditions and introduces misleading attitude such as softening when transverse deflection increases, while proposed model based on analytical solution of a buckling tends to stiffen. In other words, the proposed model comprises the stiffness change according to different applied loads and displays the negative stiffness characteristics of the buckling beam.

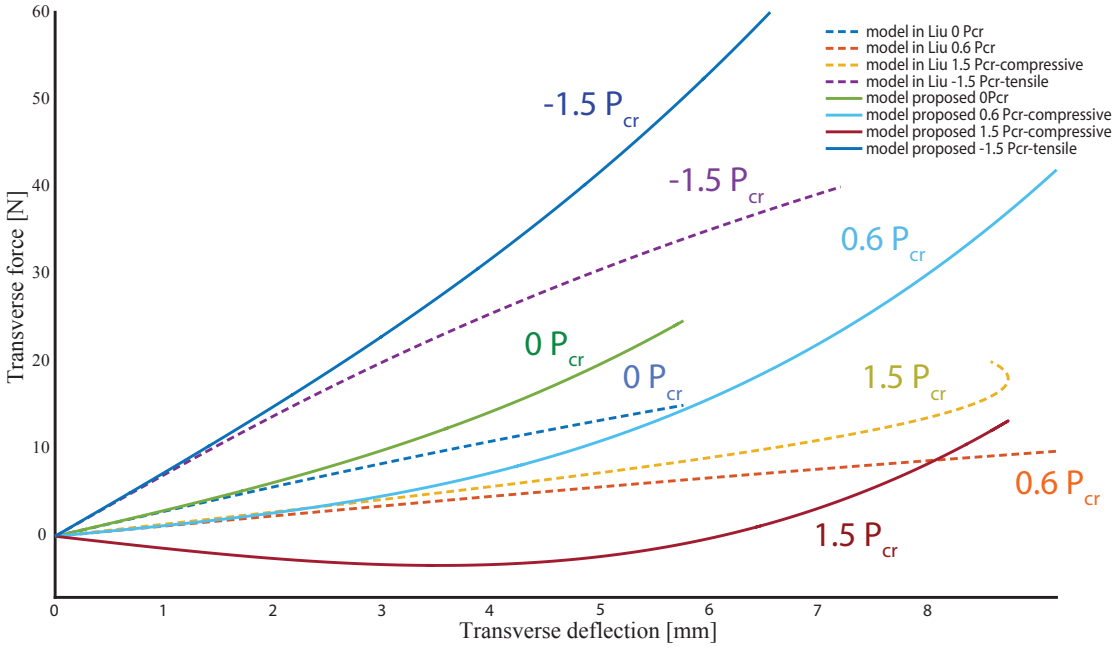

FIGURE 5.7: Comparison of the pseudo rigid body model in [3] and the proposed model based on analytical solution of a buckling beam

Chapter 6

Implementation and Characterization of Variable Stiffness Stylus

This chapter details the implementation of the variable stiffness stylus, instrumentation for experimental verification and characterization of each of its compliant elements. Two prototypes are presented.

6.1 Implementation of the Variable Stiffness Mechanism

Figure 6.1 presents two functional prototypes of the variable stiffness stylus, where the Prototype 2 is an enhanced version of the mechanism in terms of its stiffness range and size.

Both prototypes consist of compliant parallelogram joints, cross flexure joints, a buckling beam and a manually adjustable pre-tensioning mechanism. The pre-tensioning mechanism includes a screw, a compression spring, and connection parts between them. Metric 4 screws with 0.7 mm pitch are attached in order to apply pretension through rotation. The connection part between the screw and the compression spring include a Metric 4 nut and a 6800-ZZ ball bearing inside to translate the rotational motion of the screw into linear motion. The compression springs are the main source of pre-tension and are chosen to have a stiffness rate of 4.51 N/mm.

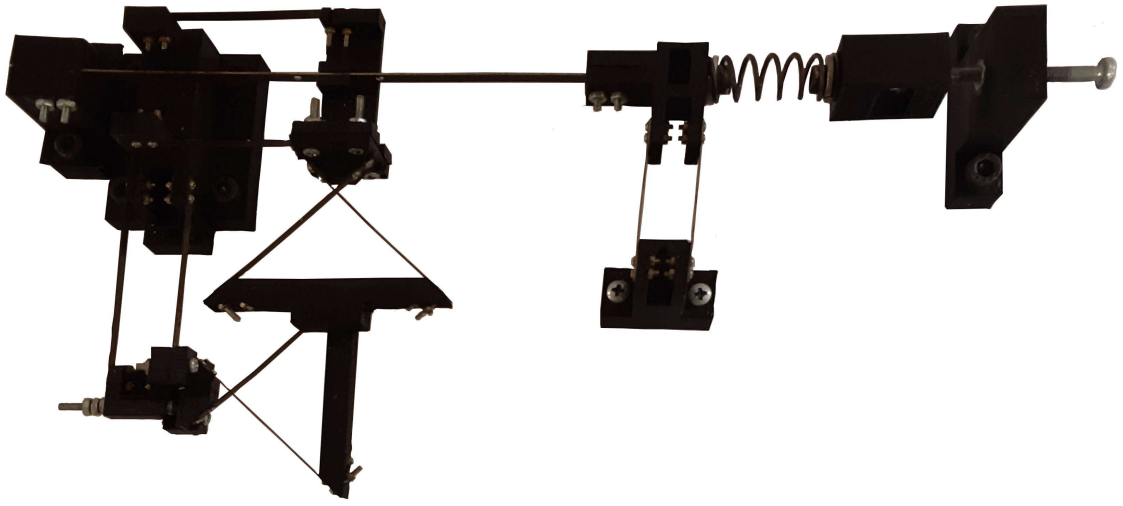

(a) First prototype

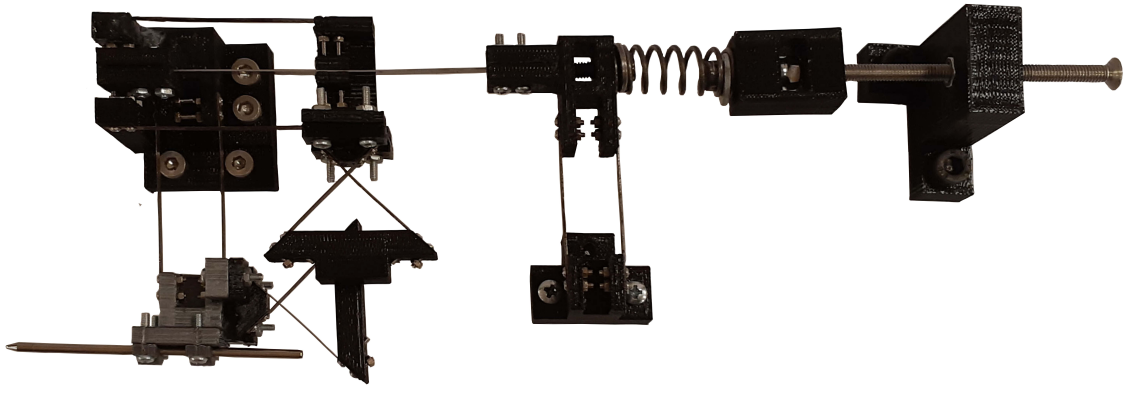

(b) Second prototype

FIGURE 6.1: Passively modifiable variable stiffness mechanism prototypes

The parallelogram joint between the compression spring and the buckling beam is implemented to ensure the guided linear motion of the beam, preventing undesired rotations. Table 6.1 lists relevant physical parameters that are used to implement both prototypes.

TABLE 6.1: Physical parameters of both prototypes

	Parameter	Prototype 1	Prototype 2
	Overall length [mm]	214.6895	168.3868
	Overall width [mm]	119.60	83.9178
	Stiffness range [N/mm]	0.0775-0.8062	0.0682-1.9871
1st Parallelogram joint beam	height [mm]	4	3
	width [mm]	0.2	0.2
	length [mm]	55	50
2st Parallelogram joint beam	height [mm]	4	3
	width [mm]	0.2	0.2
	length [mm]	50	55
Cross joint beam	height [mm]	3	3
	width [mm]	0.2	0.2
	length [mm]	50	36
Buckling beam	height [mm]	4	3
	width [mm]	0.5	0.4
	length [mm]	140	96
Prevention Parallelogram joint beam	height [mm]	3	3
	width [mm]	0.5	0.5
	length [mm]	41	41

As presented in Table 6.1, the stiffness range of Prototype 2 is significantly higher than that of Prototype 1, while its overall length and width are also reduced. Please note that the overall length of the prototypes is calculated without the tensioning screw and stylus tip, as these parts may be replaced by various other parts for different tasks.

Buckling beam is the critical part of the design because it modulates the overall stiffness through both its variable stiffness characteristics. Consequently, the dimensions of the buckling beam dominates the design decisions. If its length increases, then the first critical buckling load of the beam decreases and small axial forces can be applied to exceed this critical load and achieve negative stiffness from the beam. However, the stiffness range also diminishes, while low stiffness values can be acquired. On the other hand, if the thickness increases, then the first critical buckling load increases significantly and wider stiffness ranges can be obtained. However, higher axial forces are required applied in order to reach the first critical buckling load. For this purpose, stiffer pre-tensioning springs or bigger screws need to be placed, extending the size of the mechanism. Accordingly, the buckling beams of the styli are designed iteratively, considering the tradeoff between stiffness range and the overall device size.

The compliant power transmission mechanism rotates the tip motion by a right angle and allows the buckling beam to be placed parallel to the tip. This mechanism consists of two parallelogram joints and two cross flexure joints.

Our current implementation is based on rapid prototyping plastic parts and attaching metal beams via fasteners to form the compliant joints, as shown in Figure 6.2. All plastic connection parts are printed from PLC using a 3D printer (Makerbot Replicator 5th generation). Spring steel (AISI 1075) is preferred for beams of both cross flexure and parallelogram joints, because of its favorable deflection characteristics. This still has a high yield strength that allows the spring steel to maintain its

original shape regardless of significant twisting and deflection. The buckling beam and all other beams used for implementation of compliant joints are cut via water

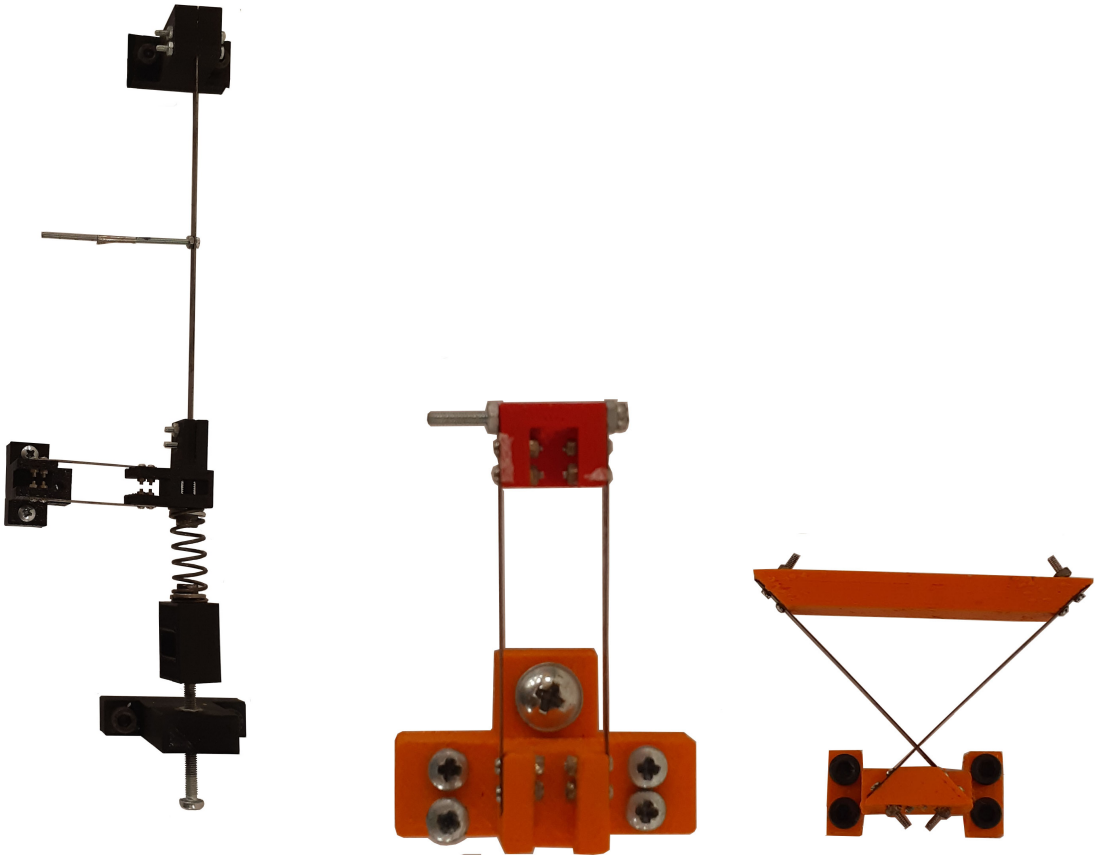

(a) Buckling beam with the pretensioning mechanism

(b) Compliant parallelogram joint

(c) Cross flexure joint

FIGURE 6.2: Implementation of compliant elements

The first parallelogram joint attached to the stylus tip has a significant effect on overall stiffness and size. Accordingly, the height, length and attachment location of this joint have been revised in Prototype 2. In particular, the height is reduced from 4 mm to 3 mm, while the link lengths are decreased from 55 mm to 50 mm to result in a more compact design with a larger stiffness range. Furthermore, the

cross flexure joints are scaled to be smaller in Prototype 2, in order to save further space. Note that apart form our current implementation based on rapid prototyping plastic parts and attaching metal beams via fasteners, it is possible to miniaturize both joints and fabricate them through alternative manufacturing methods.

6.2 Experimental Setup

Experimental setup used for the characterization of the variable stiffness stylus is presented in Figure 6.3. This setup consists of an optical encoder (US Digital EM1 with 2000 counts/inch resolution under quadrature decoding), a force sensor (ATI Nano 25) with 1/16 N resolution attached to a linear slider to apply to the tip and measure the applied force and a PC based I/O interface (Quanser Q8-USB) for real-time data acquisition. In order to acquire stiffness estimates of the variable stiffness stylus, the tip is repeatedly pressed with the force sensor and displacement versus applied force data are collected. The stiffness is estimated through the slope of a least squares line fit to this data. Each component of the variable stiffness stylus is initially isolated, then characterization is conducted through the same procedure

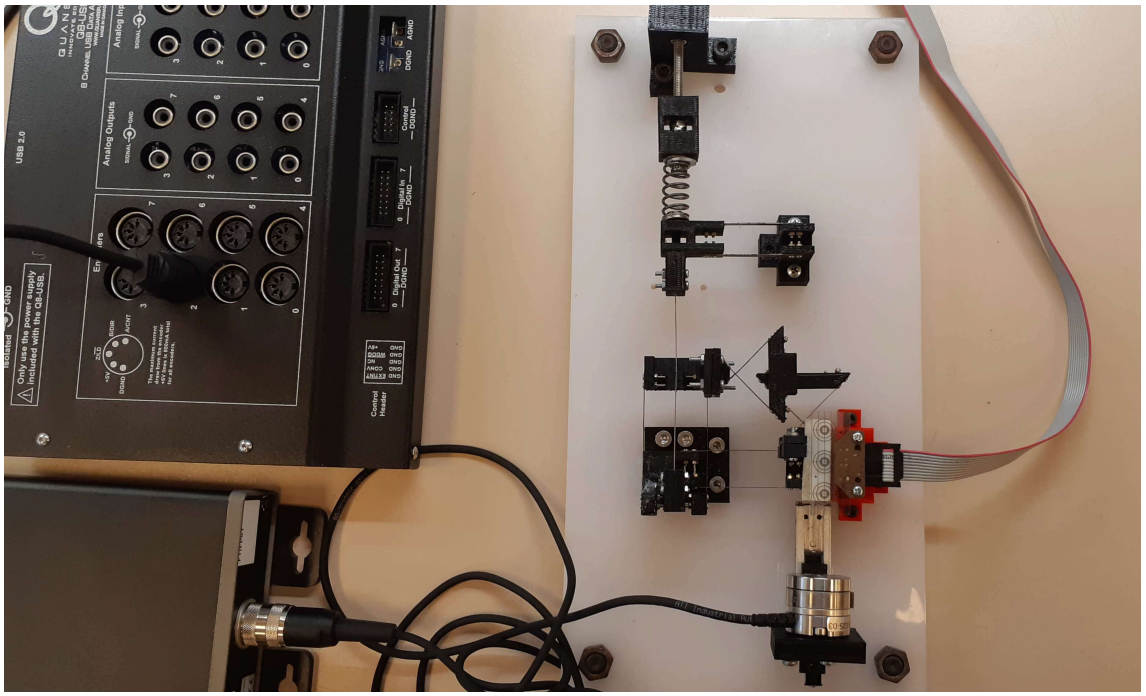

FIGURE 6.3: Experimental setup used for the characterization of the variable stiffness mechanism

6.3 Characterization Results

In order to characterize the compliant elements and validate the results of the analytical models, a set of experiments are carried out. Experimental characterization is performed by applying axial forces to the tip of the stylus, to the middle of the buckling beam and to the body of other compliant joints. Forces are applied by pressing force sensor that is rigidly attached to a linear slider. During force measurements, the displacements of the elements are recorded by encoder. After saving both values, force versus displacement graphs are plotted and least square linear fits are implemented. Each experiment is repeated at least ten times to obtain more robust experimental data. This section presents the experimental characterization results for each compliant element.

6.3.1 Cross Flexure Joint

Figure 6.4 presents experimental data collected to characterize rotational stiffness of the cross flexure joints and compare it with the analytical solution acquired from Eqn. 4.6. Due to the oscillatory characteristics of the cross flexure joints, the experimental data includes some fluctuations but this phenomenon does not significantly affect the evaluation of rotational stiffness. The red line represents the best line fit, for which R^2 is 0.9507, while yellow line is according to the analytic rotational stiffness model. From the analytical solution, a stiffness of 59.3233 Nmm/rad is expected and 59.7329 Nmm/rad is characterized through the moment-angular displacement relationship of experimental data, resulting in 0.69% RMS error.

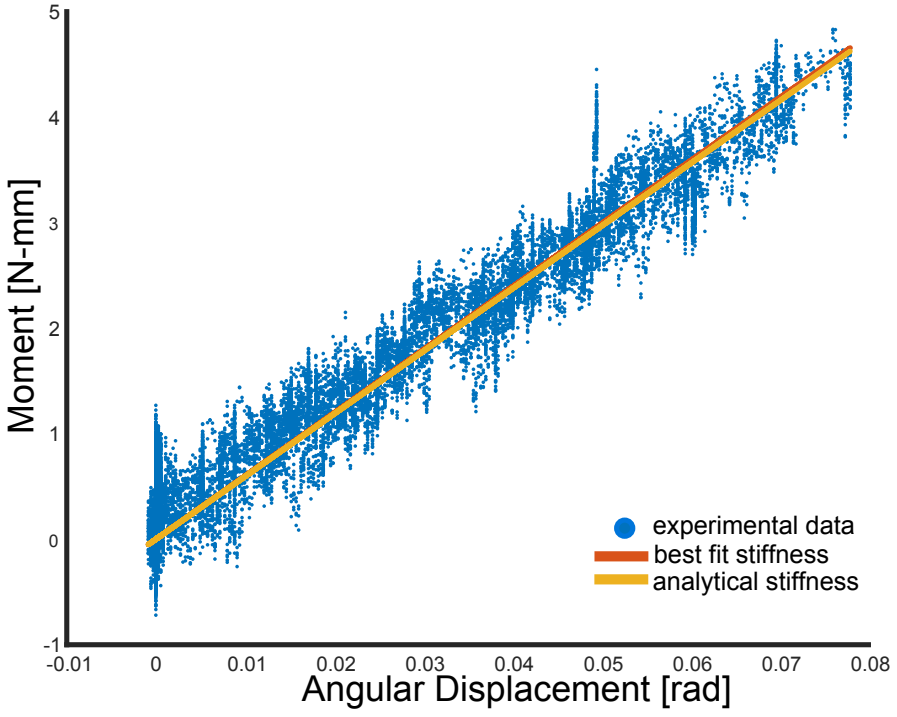

FIGURE 6.4: Characterization of cross flexure joint

6.3.2 Parallelogram Joint

Figure 6.5 presents the experimental data collected for the characterization of the parallelogram joint, and the best line fit with R^2 0.99. In particular, the analytical stiffness calculated according to Eqn. 4.5 is depicted with the yellow line, while the red line represents the best fit line. The experimental results verifies the accuracy of analytical results, with an 0.47% RMS error.

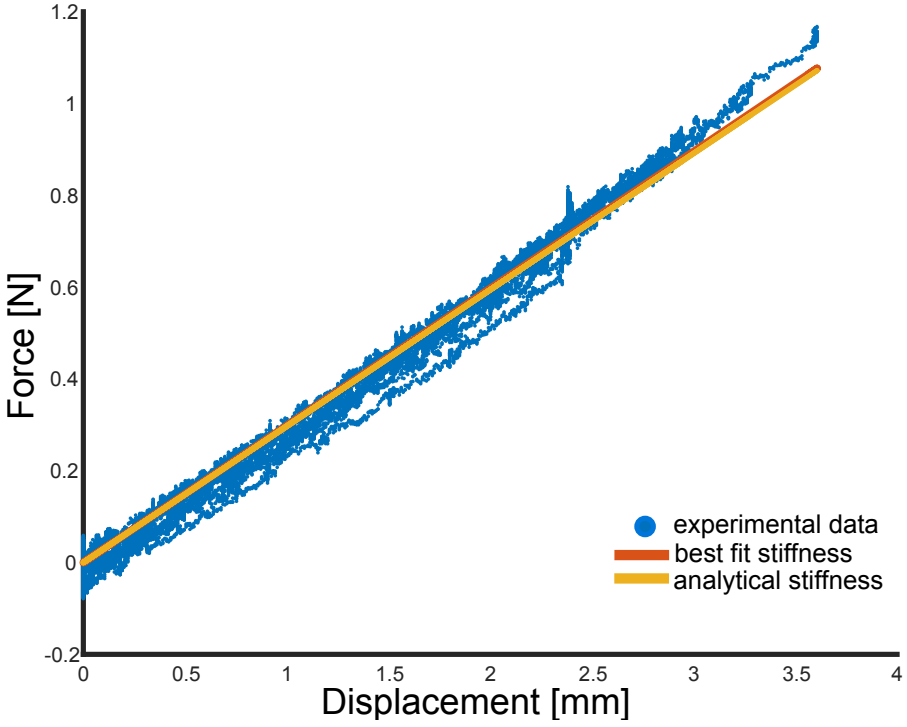

FIGURE 6.5: Characterization of parallelogram joint

6.3.3 Buckling Beam

Characterizations are performed for the buckling beam under different axial loading conditions: no load, $0.51Pcr$, $-0.51Pcr$. The results are depicted in Figures 6.6- 6.8. In particular, the experiments are conducted by adjusting the screw displacement to apply the desired axial load on the buckling beam, such that $0.51Pcr$ load is achieved by implementing 4 turns along the compression direction, while $-0.51Pcr$ is achieved by implementing 4 turns along the tensile direction. Negative sign represents tensile force. The results under these three different load conditions fit well with the analytical solution with a RMS error less than 1.7%.

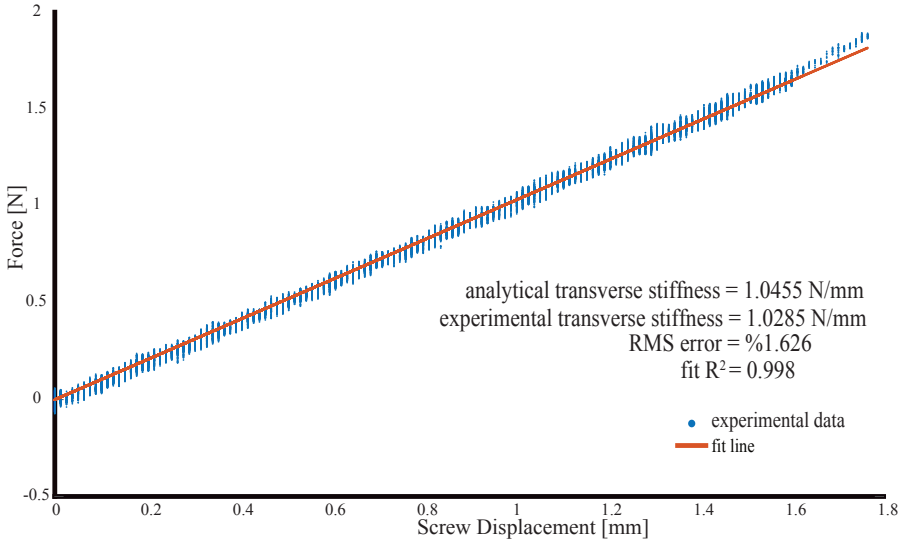

FIGURE 6.6: Characterization of buckling the beam under no axial loading

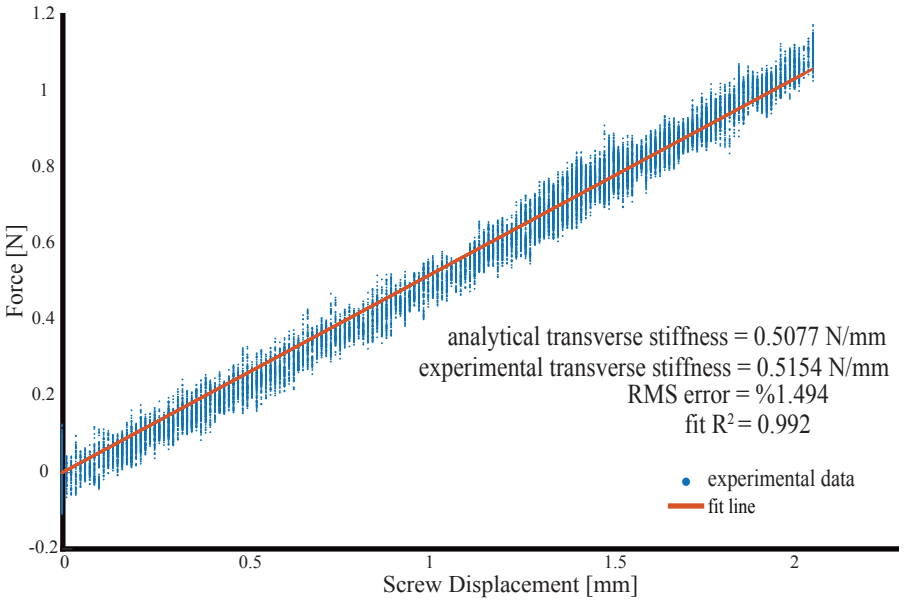

FIGURE 6.7: Characterization of buckling beam under 0.51 Pcr axial loading (compressive load)

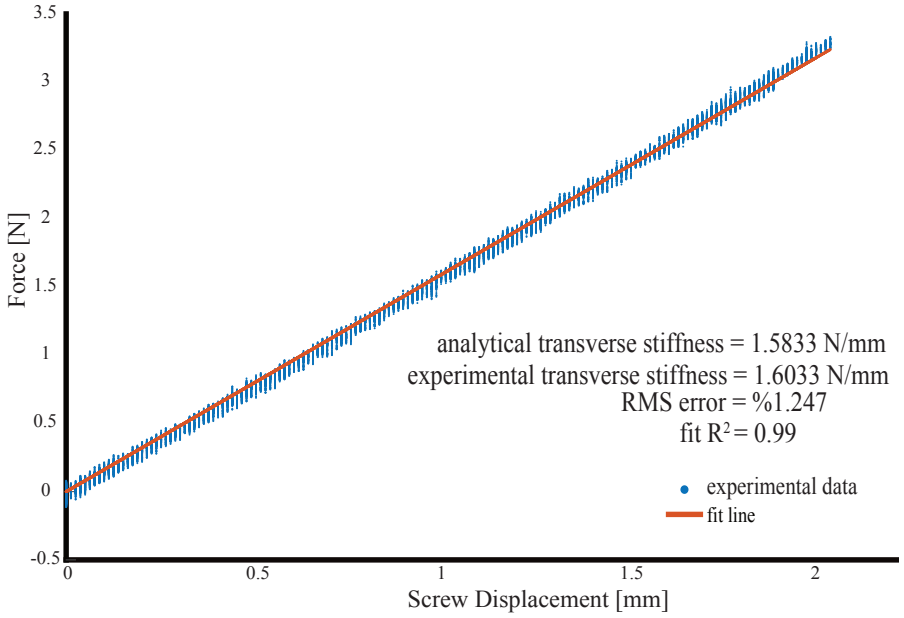

FIGURE 6.8: Characterization of buckling beam under −0.51 Pcr axial loading (tensile load)

6.3.4 Prototype 1

Figure 6.9 presents the correlation between tip stiffness and screw displacement that adjusts axial loading. The experimental data for each screw displacement is acquired through applying the same experiment procedure as before. Overall, the tip stiffness can be modulated between 0.0775 N/mm and 0.8062 N/mm. When there is no axial loading , the tip stiffness is 0.5838 N/mm. The stiffness of 0.0775 N/mm is achieved through the negative stiffness characteristics of buckling beam. In particular, after 7 turns of a metric 4 screw with a 0.7 pitch 4.9 mm displacement is achieved, that exceeds the first buckling load of the beam. At this point the negative stiffness characteristics of the beam can be observed. This phenomenon has a significant effect on the reduction of the overall stiffness below the nominal level of 0.5838N/mm which is dictated by the flexure joints. In order not to exceed the second buckling load, the axial displacement is limited to 5.6 mm.

On the other hand the overall stiffness increases up to 0.8062 N/mm. The experiments verify the tip stiffness Prototype 1 is in good agreement with the analytical solution, with average error 1.079% between -3.5 mm and 10.5 mm along the compression direction. The maximum RMS error between the analytical model and experimental characterization is recorded as 5.3%.

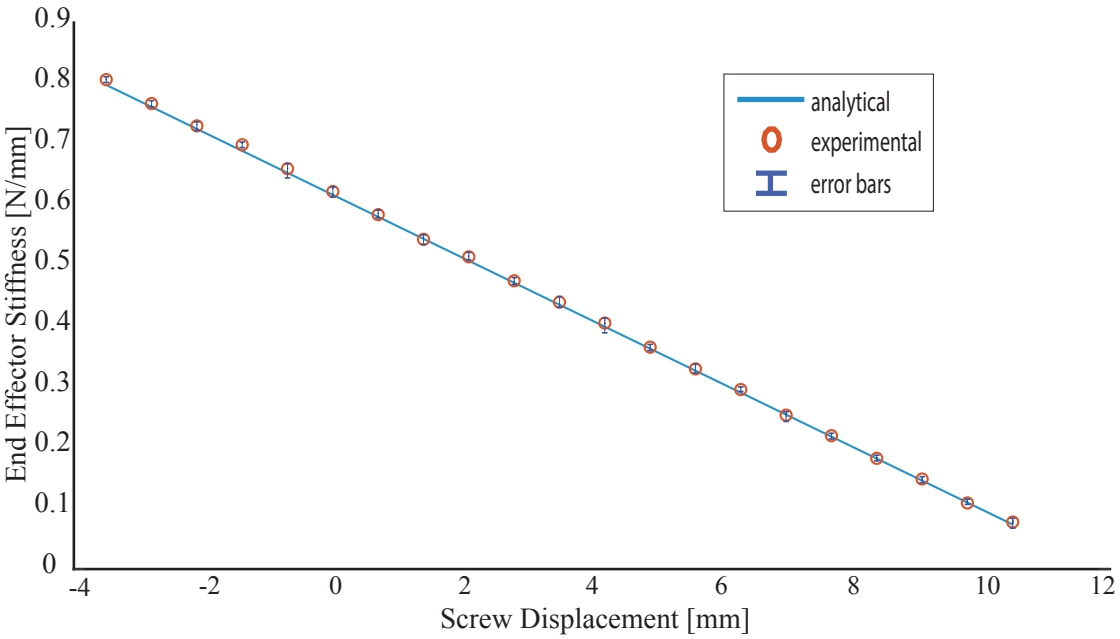

FIGURE 6.9: Characterization of the Prototype 1

6.3.5 Prototype 2

The experimental characterization results of the improved Prototype 2 is presented in Figure 6.10. For this prototype, the overall stiffness can be modulated between 0.0682 N/mm and 1.9871 N/mm. The overall stiffness modulation capability is significantly increased with the second prototype. While no axial force is applied, the tip stiffness is 1.3138 N/mm. A stiffness level of 0.0628 N/mm is achieved through the negative stiffness characteristics of buckling beam with an acceptable error level. In particular, after 6.3 mm of screw displacement, the compression force exceeds the first buckling load of the beam and the negative stiffness characteristics can be observed. This phenomenon has a significant effect on the reduction of the overall stiffness below the level 1.3138N/mm that is dictated by the flexure joints. In order not to exceed the second buckling load, the maximum rotation is limited to rotated 9.1 mm along the compression direction. On the other hand, the overall tip stiffness

can increase up to 1.9871 N/mm. Axial force can be increased; however the system exhibits larger error under high tensile loading. These experiments verifies that the tip stiffness of the Prototype 2 is in good agreement with the analytical solution, with average error of 0.8341% for axial displacements of −5.6 mm to 10.5 mm along the compression direction. The maximum RMS error between the analytical model and the experimental characterization is recorded as 4.8172%.

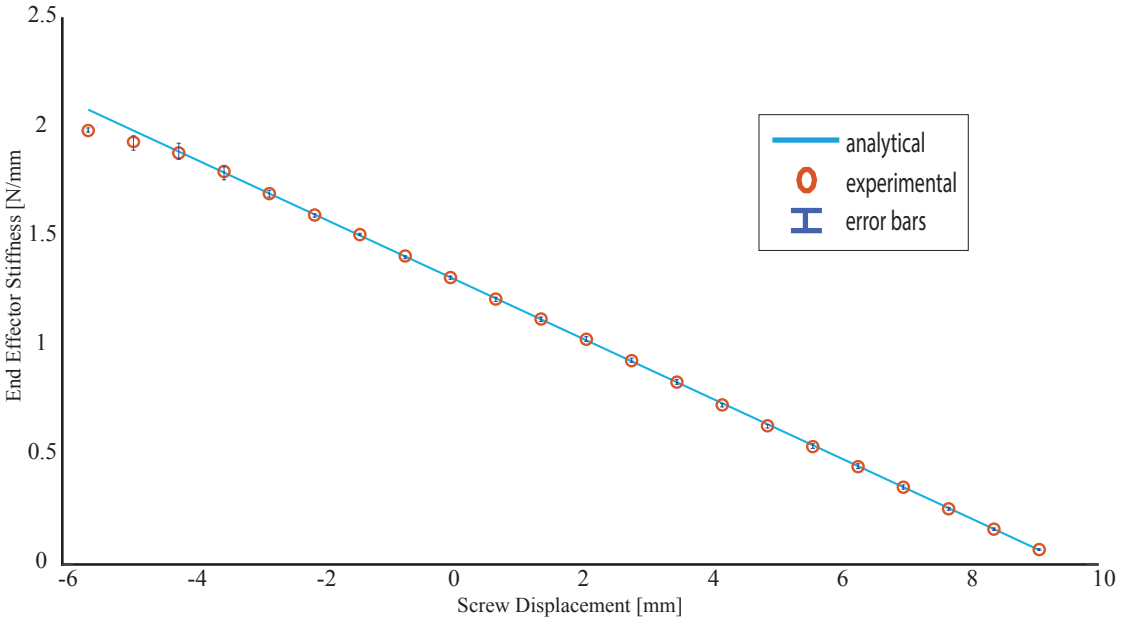

FIGURE 6.10: Characterization of the Prototype 2

6.4 Discussion

Both prototypes of the variable stiffness stylus and each compliant component that constitute the system are experimentally verified through a characterization procedure. All results are presented with an average error and the worst case error. Error bars in 6.9 and 6.10 represent the repeatability of the mechanism that experimental data for each screw displacement value is similar and there exist a little difference between higher and lower values correspond to each screw displacement. In sum, the results indicate that there exists a good agreement between analytical model and experimental characterization results for both prototypes and the compliant elements.

Moreover, the stiffness modulation characteristics of the variable stiffness stylus has been improved with the Prototype 2, while overall size has also been reduced. In other words, the stiffness rendering ranges are increased such that the stiffness of Prototype 1 can be adjusted 10 times the lowest stiffness between 0.0682 N/mm - 1.9871 N/mm while the stiffness of Prototype 2 can be adjusted 30 times its lowest stiffness value between 0.0.775 N/mm - 0.8062 N/mm.

Chapter 7

Human Subject Experiments

This chapter presents a set of human subject experiments designed to evaluate the efficacy of the manually modulated stylus stiffness on the human performance.

The human subject experiments are designed to investigate the following question: Does manually controlled variable stiffness stylus improve the human performance during various tasks with different requirements?

7.1 Experimental Setup

Figure 7.1 presents the experimental setup. The experimental setup consists of a touch screen tablet (Wacom Bamboo CTH 460), the variable stiffness stylus and a flat screen monitor. The touch screen tablet can detect 1024 levels of pressure. The stiffness of the stylus is modulated manually through rotating a screw at the end of the stylus. By adjusting the screw displacement, desired axial force on the beam is controlled and three different level of stiffness is implemented for all tasks. During the experiments, the stiffness values are set between 0.20–0.40 N/mm for *low*

stiffness, 1.10–1.30 N/mm for *intermediate stiffness* and 1.65–1.85 N/mm for *high stiffness* conditions.

For the drawing tasks, Autodesk Sketchbook is used to capture tablet data and to display it. Participants are presented with visual feedback on a flat screen monitor.

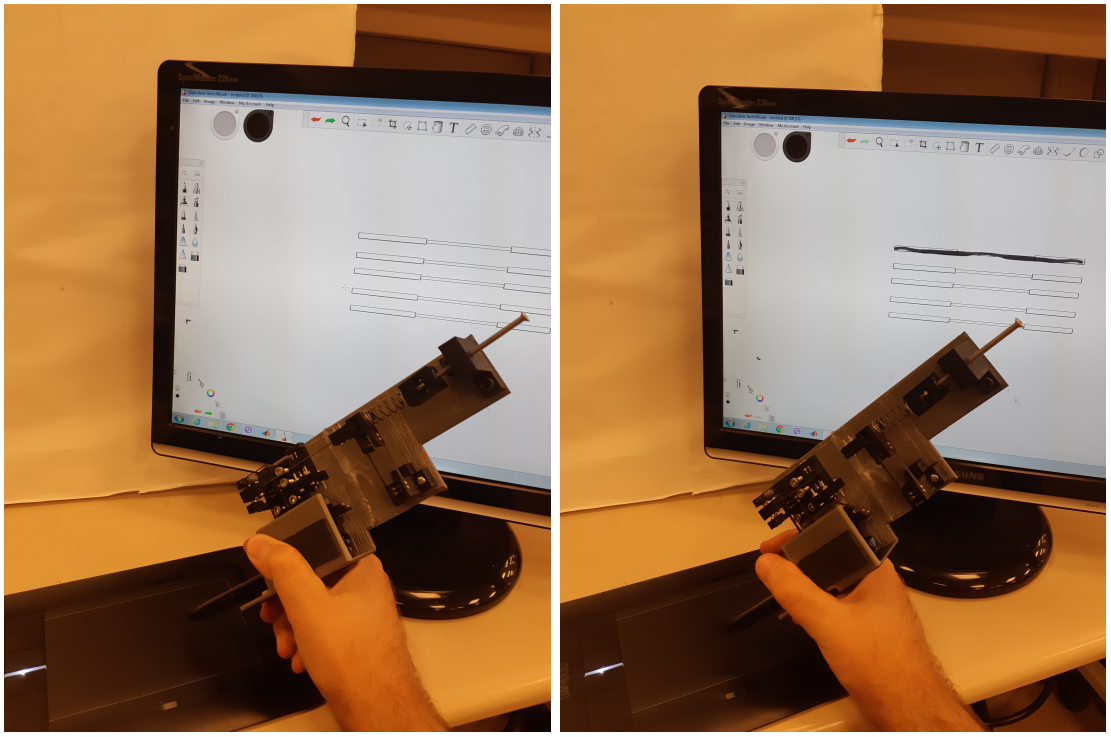

(a) Before task (b) During task

FIGURE 7.1: Experimental setup consists of the variable stiffness stylus, pressure sensitive Wacom tablet, Autodesk Sketchbook environment and a flat screen monitor

7.2 Participants

Twelve volunteers with ages between 20 to 35 participated in the experiment. No participant had any motor or sensory impairment. All participants had prior experience with interactions that include styli and touch screens. All participants signed an informed consent approved by IRB of Sabanci University.

7.3 Tasks

Participants were asked to complete three tasks:

(1) *Precise path tracking task* in which the aim is to follow predetermined paths that are constructed using several straight lines.

(2) *Force regulation task* in which the goal is to keep the stylus pressure constant while following predetermined paths with different line thickness.

(3) *Hybrid path tracking and force regulation task* in which the aim is to follow predefined paths and control the pressure, simultaneously as the thickness of the lines are also changing as one proceeds with the path.

Figure 7.2 presents screenshots for the experimental tasks that have different stiffness requirements.

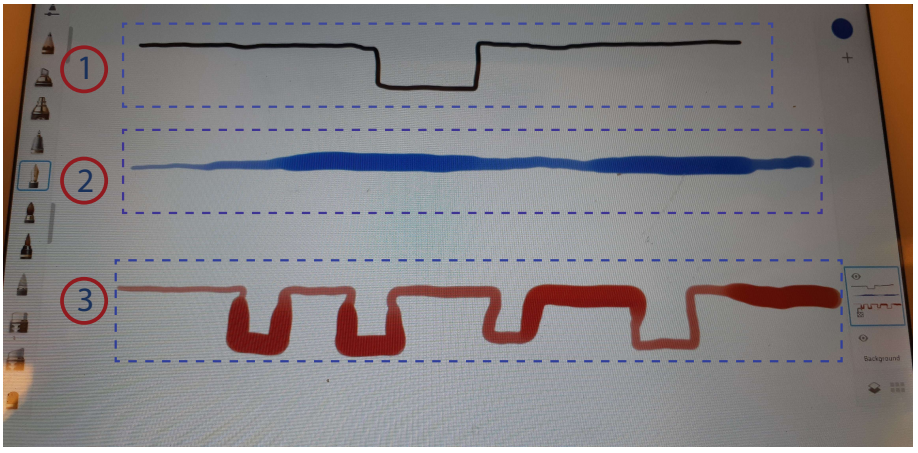

FIGURE 7.2: Three different tasks used in the experiments: (1) Precise path tracking task, (2) Force regulation task, and (3) Hybrid path tracking and force regulation task

We hypothesize that the participants will perform significantly better with different stylus stiffness levels while performing different tasks.

In literature, some systematic experiments with variable impedance modulation have been conducted in [5, 66] in the context of hand prostheses, which provide evidence that tool impedance modulation is beneficial for task performance.

Unlike the case in [5] where the experiments are performed in virtual reality, in our experiments, the participant physically hold the variable stiffness stylus as a tool than acts as an extension of their body; hence, our test conditions are provide the actual physical conditions of interaction with the touch screens.

7.4 Experimental Procedure

Before the experiment, participants were informed about the purpose of the study and instructed to ensure that they are comfortable during holding the stylus. Following the instructions, they attended an unrecorded session for 300 seconds in order to familiarize themselves with the variable stiffness stylus and interacting with the touch screen using three different levels of stylus tip stiffness. Since the stiffness levels are much above just notifiable difference, it was verified that the participants could easily perceive the current stiffness level of the stylus tip. Participants always interacted with the tablet by holding the stylus with their dominant hand. In order to minimize the distractibility, participants wore headphones playing pink noise and had a break for about 60 seconds between each session. The break period was increased as necessary, upon the participant's request.

Experimental procedure is presented in 7.3. The experiment consists of 3 sessions, while each session is composed of 3 subsessions and each subsession involves 5 trials. For each session, the tip stiffness of the stylus is set to one of the *low stiffness* (LS), *intermediate stiffness* (IS), and *high stiffness* (HS) levels. All three tasks (T1–T3) are presented to the participants during a session, in a randomized order. Each task is repeated 5 times during the trials.

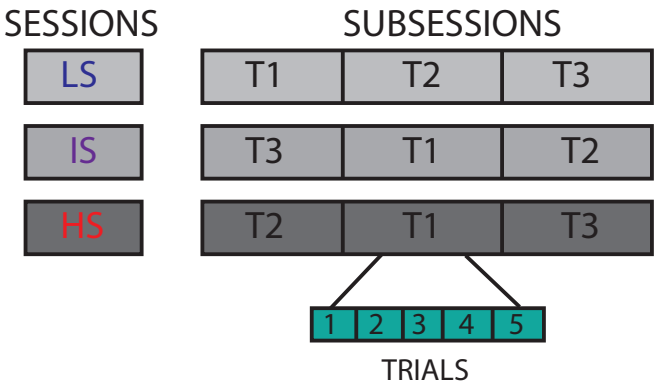

FIGURE 7.3: Schematic representation of the experimental design. The experiment consists of 3 sessions, while each session is composed of 3 subsessions and each subsession involves 5 trials. For each session, the tip stiffness of the stylus is set to one of the *low stiffness* (LS), *intermediate stiffness* (IS), and *high stiffness* (HS) levels. All three tasks (T1–T3) are presented to the participants during a session, in a randomized order. Each task is repeated 5 times during the trials.

7.5 Performance Metrics

For the precise path tracking task, a performance metric is determined by the RMS path error which captures the deviations from the predefined path. Subjects draw their lines on the predefined path that consists of straight lines and this lines are partitioned into straight line segments and digitalized in order to implement linear curve fits to them. The quality of the linear fit determined by R^2 and RMS error are used to quantify the match between user-drawing and predefined lines.

For the force regulation task, pressure level is selected as a performance metric. The tablet environment is sensitive to pressure differences and thickness of the lines change according to these pressure levels, that is, the more pressure is applied to the Wacom tablet, the thicker lines are produced. In order to determine the pressure levels during the force regulation task, black pixels inside the predefined line thickness are counted, instead of capturing the pressure data directly. The metric is preferred to be defined over the line output, as this metric directly relates to the

task of drawing lines of constant thickness, while there exists a mapping between the raw pressure data and the line thickness determined by the drawing software.

For the hybrid path tracking and force regulation task, both metrics defined above are employed.

Furthermore, task completion times are recorded as a secondary quantitative metric.

For qualitative evaluations, the participants were asked to fill in a short questionnaire that aims to determine their tip stiffness preferences for each task. In particular, after the experiments, the participants ranked their tip stiffness preferences for each task in such a way that, where 1 denotes "more comfortable- first choice" and 3 denotes "less comfortable – third choice".

7.6 Expected Results

We hypothesize that participants will perform better in the precise path tracking task using the high stiffness configuration, in the force regulation tracking task using the low stiffness configuration, and in the hybrid task using the intermediate stiffness configuration.

7.7 Analysis of Results

A repeated measures ANOVA will be employed to determine the significance of the stylus tip stiffness on task performance, while post-hoc analysis will be performed to compare the performance differences among the tip stiffness levels.

7.8 Discussion

Human experiments are currently ongoing; hence, experimental results could not be included in the thesis due to strict deadlines enforced to submit the thesis. The results of the human subject experiments is planned to be published as soon as the experiments and their analyses are completed.

Chapter 8

Conclusion

A novel compliant stylus with manually adjustable tip stiffness has been proposed. Two prototypes of the stylus have been implemented based on various compliant elements to feature stiffness ranges. Stiffness modulation capabilities of both prototypes have been experimentally characterized. Thanks to the variable stiffness characteristics of axially loaded buckling beams, very low stiffness levels around 0.07 N/mm has been achieved without sacrificing the mechanical integrity and load bearing capacity of the stylus.

The design inherits the advantages of compliant mechanisms In particular, the compliant design ensures that the stylus does not exhibit parasitic effects such, as friction, stiction, wear and backlash. The compliant stylus is analysed through pseudo rigid modeling technique, an efficient method for modeling flexible elements undergoing nonlinear behaviour due to the large deflections. The characterization results indicate that stiffness characteristics of the prototypes have been matched with the predictions based on the analytical stiffness derivations.

In order to effectively model fixed guided beams that undergo transverse stiffness variations around their first critical buckling load, a novel pseudo rigid body model

has been derived. This novel equivalent pseudo rigid body model for fixed guided beams is based on the analytical solution of buckling beams. Under different axial loading conditions, the model has been experimentally verified to have less than %3 error.

Human subject experiments have been conducted for the purpose of evaluating the impact of the manually modulated stylus stiffness on the human performance during physical interactions with the environment. In particular, human performance for three tasks with different requirements such as high position control, force regulation and composition of both position control and force regulation have been tested.

Future works include design optimization of the novel compliant stylus to achieve an ideal compromise between the device size and its stiffness range. Furthermore, the size can be reduced by alternative manufacturing techniques including micro-machining and electrical discharge machining.

Bibliography

[1] L. L. Howell, "Compliant mechanisms," 2001.

[2] A. Midha, S. G. Bapat, A. Mavanthoor, and V. Chinta, "Analysis of a fixed-guided compliant beam with an inflection point using the pseudo-rigid-body model concept," *Journal of Mechanisms and Robotics*, vol. 7, no. 3, p. 031007, 2015.

[3] P. Liu and P. Yan, "A modified pseudo-rigid-body modeling approach for compliant mechanisms with fixed-guided beam flexures," *Mechanical Sciences*, vol. 8, no. 2, pp. 359–368, 2017.

[4] T. A. Carlson, G. Alvarez, D. an Wu, and F. A. Verstraten, "Rapid assimilation of external objects into the body schema," *Psychological Science*, vol. 21, no. 7, pp. 1000–1005, 2010.

[5] A. Blank, A. Okamura, and L. Whitcomb, "Task-dependent impedance improves user performance with a virtual prosthetic arm," in *IEEE Int. Conference on Robotics and Automation*, pp. 2235–2242, 2011.

[6] A. Blank, A. Okamura, and L. Whitcomb, "User comprehension of task performance with varying impedance in a virtual prosthetic arm: A pilot study," *IEEE International Conference on Biomedical Robotics and Biomechatronics*, pp. 500–507, 2012.

[7] A. Blank, A. Okamura, and L. Whitcomb, "Task-dependent impedance and implications for upper-limb prosthesis control," *International Journal of Robotics Research*, vol. 3, no. 6, pp. 827–846, 2013.

[8] E. Hocaoglu and V. Patoglu, "Design, implementation and evaluation of a variable stiffness transradial hand prosthesis," *IEEE/ASME Transactions on Mechatronics*. (under review).

[9] J. C. Lee, P. H. Diets, D. Leigh, W. S. Yerazunis, and S. E. Hudson, "Haptic pen: Tactile feedback stylus for touch screens," in *ACM Symposium on User Interface Software and Technology*, 2004.

[10] P. Dietz, D. Leigh, W. Yerazunis, and J. Lee, "Hand-held haptic stylus," Nov. 10 2005. US Patent App. 10/840,748.

[11] M. Fiorentino, A. E. Uva, and G. Monno, "The senstylus: A novel rumble-feedback pen device for cad application in virtual reality," in *International Conference in Central Europe on Computer Graphics, Visualization and Computer Vision*, 2005.

[12] K. U. Kyung and J. Y. Lee, "Ubi-pen: A haptic interface with texture and vibrotactile display," *IEEE computer graphics and applications*, vol. 29, no. 1, 2009.

[13] K.-U. Kyung, J.-Y. Lee, J. Park, and M. A. Srinivasan, "wubi-pen: Sensory feedback stylus interacting with graphical user interface," *Presence: Teleoperators and Virtual Environments*, vol. 21, no. 2, pp. 142–155, 2012.

[14] A. Arasan, C. Basdogan, and T. M. Sezgin, "Haptistylus: A novel stylus for conveying movement and rotational torque effects," *IEEE Computer Graphics and Applications*, vol. 36, no. 1, pp. 30–41, 2016.

[15] Y. Cho, A. Bianchi, N. Marquardt, and N. Bianchi-Berthouze, "Realpen: Providing realism in handwriting tasks on touch surfaces using auditory-tactile

feedback," in *Proceedings of the 29th Annual Symposium on User Interface Software and Technology*, pp. 195–205, 2016.

[16] A. Withana, M. Kondo, Y. Makino, G. Kakehi, M. Sugimoto, and M. Inami, "Impact: Immersive haptic stylus to enable direct touch and manipulation for surface computing," *ACM Computers in Entertainment*, vol. 8, no. 2, 2010.

[17] S. Nagasaka, Y. Uranishi, S. Yoshimoto, M. Imura, and O. Oshiro, "Haptylus: Haptic stylus for interaction with virtual objects behind a touch screen," in *SIGGRAPH Asia 2014 Emerging Technologies*, pp. 9:1–9:3, 2014.

[18] S. Kamuro, K. Minamizawa, N. Kawakami, and S. Tachi, "Ungrounded kinesthetic pen for haptic interaction with virtual environments," in *IEEE International Symposium on Robot and Human Interactive Communication*, 2009.

[19] G. Wintergerst, R. Jagodzinski, F. Hemmert, A. Muller-Rakow, and G. Joost, "Reflective haptics: Enhancing stylus-based interactions on touch screens," vol. 6191, pp. 360–366, 2010.

[20] S. Adhikari, "Stylus based haptic peripheral for touch screen and tablet devices," Mar. 25 2014. US Patent 8,681,130.

[21] S. B. Schorr, Z. F. Quek, R. Y. Romano, I. Nisky, W. R. Provancher, and A. M. Okamura, "Sensory substitution via cutaneous skin stretch feedback," in *2013 IEEE International Conference on Robotics and Automation*, pp. 2341–2346, 2013.

[22] R. Lyu, H. Hao, W. Chen, Y. Liu, F. Wang, and A. C. H. Wu, "Elastylus: Flexible haptic painting stylus," in *SIGGRAPH Asia 2015 Emerging Technologies*, pp. 10:1–10:3, 2015.

[23] T. Lyyra, J. Jurvelin, P. Pitkänen, U. Väätäinen, and I. Kiviranta, "Indentation instrument for the measurement of cartilage stiffness under arthroscopic control," *Medical engineering & physics*, vol. 17, no. 5, pp. 395–399, 1995.

[24] F. J. Carter, T. G. Frank, P. J. Davies, D. McLean, and A. Cuschieri, "Measurements and modelling of the compliance of human and porcine organs," *Medical Image Analysis*, vol. 5, no. 4, pp. 231–236, 2001.

[25] M. Ottensmeyer, "Tempest i-d: an instrument for measuring solid organ soft tissue properties," *Experimental Techniques*, vol. 26, no. 3, pp. 48–50, 2002.

[26] J. P. Arokoski, J. Surakka, T. Ojala, P. Kolari, and J. S. Jurvelin, "Feasibility of the use of a novel soft tissue stiffness meter," *Physiological measurement*, vol. 26, no. 3, p. 215, 2005.

[27] H. Liu, J. Li, X. Song, L. D. Seneviratne, and K. Althoefer, "Rolling indentation probe for tissue abnormality identification during minimally invasive surgery," *IEEE Transactions on Robotics*, vol. 27, no. 3, pp. 450–460, 2011.

[28] S. McKinley, A. Garg, S. Sen, R. Kapadia, A. Murali, K. Nichols, S. Lim, S. Patil, P. Abbeel, A. M. Okamura, *et al.*, "A single-use haptic palpation probe for locating subcutaneous blood vessels in robot-assisted minimally invasive surgery," in *Automation Science and Engineering (CASE), 2015 IEEE International Conference on*, pp. 1151–1158, IEEE, 2015.

[29] M. H. Araghi and S. Salisbury, "A feedback based dynamic instrument for measuring mechanical properties of soft tissues for minimally-invasive surgery," *Smart Materials and Structures*, no. October, pp. 59–69, 2009.

[30] M. Jia, J. W. Zu, and A. Hariri, "A new tissue resonator indenter device and reliability study," *Sensors*, vol. 11, no. 1, pp. 1212–1228, 2011.

[31] Y. Murayama, M. Haruta, Y. Hatakeyama, T. Shiina, H. Sakuma, S. Takenoshita, S. Omata, and C. E. Constantinou, "Development of a new instrument for examination of stiffness in the breast using haptic sensor technology," *Sensors and Actuators A: Physical*, vol. 143, no. 2, pp. 430–438, 2008.

[32] N. Sornkarn, P. Dasgupta, and T. Nanayakkara, "Morphological computation of haptic perception of a controllable stiffness probe," *PloS one*, vol. 11, no. 6, p. e0156982, 2016.

[33] N. Herzig, P. Maiolino, F. Iida, and T. Nanayakkara, "A variable stiffness robotic probe for soft tissue palpation," *IEEE Robotics and Automation Letters*, vol. 3, no. 2, pp. 1168–1175, 2018.

[34] K. Bisshopp and D. Drucker, "Large deflection of cantilever beams," *Quarterly of Applied Mathematics*, vol. 3, no. 2, pp. 272–275, 1945.

[35] R. Frisch-Fay, "Flexible bars," 1962.

[36] K. Mattiasson, "Numerical results from large deflection beam and frame problems analyzed by means of elliptic integrals," *International Journal for Numerical Methods in Engineering*, vol. 17, pp. 145–153, 1981.

[37] L. Howell and A. Midha, "Parametric deflection approximations for end-loaded, large-deflection beams in compliant mechanisms," *Journal of Mechanical Design, Trans. ASME*, vol. 117, no. 1, pp. 156–165, 1995.

[38] T. Yang, "Matrix displacement solution to elastica problems of beams and frames," *International Journal of Solids and Structures*, vol. 9, no. 7, pp. 829–842, 1973.

[39] K.-J. Bathe and S. Bolourchi, "Large displacement analysis of three-dimensional beam structures," *International journal for numerical methods in engineering*, vol. 14, no. 7, pp. 961–986, 1979.

[40] L. L. Howell and A. Midha, "A method for the design of compliant mechanisms with small-length flexural pivots," *Journal of mechanical design*, vol. 116, no. 1, pp. 280–290, 1994.

[41] L. L. Howell, A. Midha, and T. Norton, "Evaluation of equivalent spring stiffness for use in a pseudo-rigid-body model of large-deflection compliant mechanisms," *Journal of Mechanical Design*, vol. 118, no. 1, pp. 126–131, 1996.

[42] M. Manuvinakurake, U. Gandhi, U. Mangalanathan, and M. Nayak, "Design, fabrication and testing of fiber bragg grating based fixed guided beam pressure sensor," *Optik*, vol. 158, pp. 1063–1072, 2018.

[43] Y. Liu, Y. Zhang, and Q. Xu, "Design and control of a novel compliant constant-force gripper based on buckled fixed-guided beams," *IEEE/ASME Transactions on Mechatronics*, vol. 22, no. 1, pp. 476–486, 2017.

[44] L. Yuanqiang and L. Wangyu, "Analysis of the displacement of distributed compliant parallel-guiding mechanism considering parasitic rotation and deflection on the guiding plate," *Mechanism and Machine Theory*, vol. 80, pp. 151–165, 2014.

[45] Y. Luo, W. Liu, and L. Wu, "Analysis of the displacement of lumped compliant parallel-guiding mechanism considering parasitic rotation and deflection on the guiding plate and rigid beams," *Mechanism and Machine Theory*, vol. 91, pp. 50–68, 2015.

[46] J. Derderian, L. Howell, M. Murphy, S. Lyon, and S. Pack, "Compliant parallel-guiding mechanisms," in *Proceedings of the 1996 ASME Mechanisms Conference*, 1996.

[47] Y. Xuefeng, L. Wei, W. Yuqiao, Z. Lili, Y. Guo, and S. Xiuping, "Analysis of the displacement of complaint double parallel four-bar mechanism," in *Industrial Electronics and Applications, 2009. ICIEA 2009. 4th IEEE Conference on*, pp. 2760–2763, IEEE, 2009.

[48] C. Kim and D. Ebenstein, "Curve decomposition for large deflection analysis of fixed-guided beams with application to statically balanced compliant mechanisms," *Journal of Mechanisms and Robotics*, vol. 4, no. 4, p. 041009, 2012.

[49] N. D. Masters and L. L. Howell, "A three degree-of-freedom model for self-retracting fully compliant bistable micromechanisms," *Journal of Mechanical Design*, vol. 127, no. 4, pp. 739–744, 2005.

[50] B. R. Cannon, T. D. Lillian, S. P. Magleby, L. L. Howell, and M. R. Linford, "A compliant end-effector for microscribing," *Precision engineering*, vol. 29, no. 1, pp. 86–94, 2005.

[51] G. Hao and H. Li, "Extended static modeling and analysis of compliant compound parallelogram mechanisms considering the initial internal axial force," *Journal of mechanisms and robotics*, vol. 8, no. 4, p. 041008, 2016.

[52] F. Ma and G. Chen, "Bi-bcm: A closed-form solution for fixed-guided beams in compliant mechanisms," *Journal of Mechanisms and Robotics*, vol. 9, no. 1, p. 014501, 2017.

[53] S. M. Lyon, "The pseudo-rigid-body model for dynamic predictions of macro and micro compliant mechanisms," 2003.

[54] J. Yamaguchi and A. Takanishi, "Design of biped walking robots having antagonistic driven joints using nonlinear spring mechanism," in *Intelligent Robots and Systems, 1997. IROS'97., Proceedings of the 1997 IEEE/RSJ International Conference on*, vol. 1, pp. 251–259, IEEE, 1997.

[55] K. Koganezawa, Y. Watanabe, and N. Shimizu, "Antagonistic muscle-like actuator and its application to multi-dof forearm prosthesis," *Advanced Robotics*, vol. 12, no. 7-8, pp. 771–789, 1997.

[56] J. Yamaguchi, D. Nishino, and A. Takanishi, "Realization of dynamic biped walking varying joint stiffness using antagonistic driven joints," in *Robotics and*

Automation, 1998. Proceedings. 1998 IEEE International Conference on, vol. 3, pp. 2022–2029, IEEE, 1998.

[57] A. Bicchi and G. Tonietti, "Fast and" soft-arm" tactics [robot arm design]," *IEEE Robotics & Automation Magazine*, vol. 11, no. 2, pp. 22–33, 2004.

[58] S. A. Migliore, E. A. Brown, and S. P. DeWeerth, "Biologically inspired joint stiffness control," in *Robotics and Automation, 2005. ICRA 2005. Proceedings of the 2005 IEEE International Conference on*, pp. 4508–4513, IEEE, 2005.

[59] G. Tonietti, R. Schiavi, and A. Bicchi, "Design and control of a variable stiffness actuator for safe and fast physical human/robot interaction," in *Robotics and Automation, 2005. ICRA 2005. Proceedings of the 2005 IEEE International Conference on*, pp. 526–531, IEEE, 2005.

[60] S. A. Migliore, E. A. Brown, and S. P. DeWeerth, "Novel nonlinear elastic actuators for passively controlling robotic joint compliance," *Journal of Mechanical Design*, vol. 129, no. 4, pp. 406–412, 2007.

[61] R. Schiavi, G. Grioli, S. Sen, and A. Bicchi, "Vsa-ii: A novel prototype of variable stiffness actuator for safe and performing robots interacting with humans," in *Robotics and Automation, 2008. ICRA 2008. IEEE International Conference on*, pp. 2171–2176, IEEE, 2008.

[62] S. Wolf and G. Hirzinger, "A new variable stiffness design: Matching requirements of the next robot generation," in *Robotics and Automation, 2008. ICRA 2008. IEEE International Conference on*, pp. 1741–1746, IEEE, 2008.

[63] F. Petit, M. Chalon, W. Friedl, M. Grebenstein, A. Albu-Schäffer, and G. Hirzinger, "Bidirectional antagonistic variable stiffness actuation: Analysis, design & implementation," in *Robotics and Automation (ICRA), 2010 IEEE International Conference on*, pp. 4189–4196, IEEE, 2010.

[64] W. Friedl, H. Höppner, F. Petit, and G. Hirzinger, "Wrist and forearm rotation of the dlr hand arm system: Mechanical design, shape analysis and experimental validation," in *Intelligent Robots and Systems (IROS), 2011 IEEE/RSJ International Conference on*, pp. 1836–1842, IEEE, 2011.

[65] M. G. Catalano, G. Grioli, M. Garabini, F. Bonomo, M. Mancini, N. Tsagarakis, and A. Bicchi, "Vsa-cubebot: A modular variable stiffness platform for multiple degrees of freedom robots," in *Robotics and Automation (ICRA), 2011 IEEE International Conference on*, pp. 5090–5095, IEEE, 2011.

[66] E. Hocaoglu and V. Patoglu, "Tele-impedance control of a variable stiffness prosthetic hand," in *IEEE International Conference on Robotics and Biomimetics*, pp. 1576–1582, 2012.

[67] S. Sugano, S. Tsuto, and I. Kato, "Force control of the robot finger joint equipped with mechanical compliance adjuster," in *Intelligent Robots and Systems, 1992., Proceedings of the 1992 lEEE/RSJ International Conference on*, vol. 3, pp. 2005–2013, IEEE, 1992.

[68] T. Morita and S. Sugano, "Design and development of a new robot joint using a mechanical impedance adjuster," in *Robotics and Automation, 1995. Proceedings., 1995 IEEE International Conference on*, vol. 3, pp. 2469–2475, IEEE, 1995.

[69] H. Seki, A. Takada, Y. Kamiya, M. Hikizu, and H. Nomura, "development of a robot joint mechanism with variable compliance by rotating a leaf spring," in *Proc. Japan/USA Flexible Automation Conf*, pp. 13019–13024, 2000.

[70] S. Kawamura, T. Yamamoto, D. Ishida, T. Ogata, Y. Nakayama, O. Tabata, and S. Sugiyama, "Development of passive elements with variable mechanical

impedance for wearable robots," in *Robotics and Automation, 2002. Proceedings. ICRA'02. IEEE International Conference on*, vol. 1, pp. 248–253, IEEE, 2002.

[71] K. Hollander and T. Sugar, "Concepts for compliant actuation in wearable robotic systems," in *US-Korea Conference (UKC) CDROM*, 2004.

[72] K. Hollander, T. Sugar, and D. Herring, "Adjustable robotic tendon using a 'jack spring'," in *IEEE International Conference on Rehabilitation Robotics*, pp. 113–118, 2005.

[73] J. Choi, S. Hong, W. Lee, S. Kang, and M. Kim, "A robot joint with variable stiffness using leaf springs," *IEEE Transactions on Robotics*, vol. 27, no. 2, pp. 229–238, 2011.

[74] J. Schuy, P. Beckerle, J. Wojtusch, S. Rinderknecht, and O. Von Stryk, "Conception and evaluation of a novel variable torsion stiffness for biomechanical applications," in *Biomedical Robotics and Biomechatronics (BioRob), 2012 4th IEEE RAS & EMBS International Conference on*, pp. 713–718, IEEE, 2012.

[75] J. M. Schimmels and D. R. Garces, "The arched flexure vsa: A compact variable stiffness actuator with large stiffness range," in *Robotics and Automation (ICRA), 2015 IEEE International Conference on*, pp. 220–225, IEEE, 2015.

[76] J. S. Sulzer, M. A. Peshkin, and J. L. Patton, "Marionet: An exotendon-driven rotary series elastic actuator for exerting joint torque," in *Rehabilitation Robotics, 2005. ICORR 2005. 9th International Conference on*, pp. 103–108, IEEE, 2005.

[77] R. Van Ham, B. Vanderborght, M. Van Damme, B. Verrelst, and D. Lefeber, "MACCEPA, the mechanically adjustable compliance and controllable equilibrium position actuator: Design and implementation in a biped robot," *Robotics and Autonomous Systems*, vol. 55, pp. 761–768, 2007.

[78] B. Vanderborght, N. G. Tsagarakis, R. Van Ham, I. Thorson, and D. G. Caldwell, "Maccepa 2.0: compliant actuator used for energy efficient hopping robot chobino1d," *Autonomous Robots*, vol. 31, no. 1, p. 55, 2011.

[79] A. Jafari, N. G. Tsagarakis, B. Vanderborght, and D. G. Caldwell, "A novel actuator with adjustable stiffness (awas)," in *Intelligent robots and systems (iros), 2010 ieee/rsj international conference on*, pp. 4201–4206, IEEE, 2010.

[80] B.-S. Kim and J.-B. Song, "Hybrid dual actuator unit: A design of a variable stiffness actuator based on an adjustable moment arm mechanism," in *Robotics and automation (icra), 2010 ieee international conference on*, pp. 1655–1660, IEEE, 2010.

[81] A. Jafari, N. G. Tsagarakis, and D. G. Caldwell, "Awas-ii: A new actuator with adjustable stiffness based on the novel principle of adaptable pivot point and variable lever ratio," in *Robotics and Automation (ICRA), 2011 IEEE International Conference on*, pp. 4638–4643, IEEE, 2011.

[82] N. G. Tsagarakis, I. Sardellitti, and D. G. Caldwell, "A new variable stiffness actuator (compact-vsa): Design and modelling," in *Intelligent Robots and Systems (IROS), 2011 IEEE/RSJ International Conference on*, pp. 378–383, IEEE, 2011.

[83] S. Rao, R. Carloni, and S. Stramigioli, "A novel energy-efficient rotational variable stiffness actuator," in *Engineering in Medicine and Biology Society, EMBC, 2011 Annual International Conference of the IEEE*, pp. 8175–8178, IEEE, 2011.

[84] M. Fumagalli, E. Barrett, S. Stramigioli, and R. Carloni, "The mvsa-ut: A miniaturized differential mechanism for a continuous rotational variable stiffness actuator," in *Biomedical Robotics and Biomechatronics (BioRob), 2012 4th IEEE RAS & EMBS International Conference on*, pp. 1943–1948, IEEE, 2012.

[85] S. S. Groothuis, G. Rusticelli, A. Zucchelli, S. Stramigioli, and R. Carloni, "The vsaut-ii: A novel rotational variable stiffness actuator," in *Robotics and Automation (ICRA), 2012 IEEE International Conference on*, pp. 3355–3360, IEEE, 2012.

[86] M. Yalcin, B. Uzunoglu, E. Altintepe, and V. Patoglu, "VnSA: Variable negative stiffness actuation based on nonlinear deflection characteristics of buckling beams," in *IEEE/RSJ International Conference on Intelligent Robots and Systems (IROS 2013)*, 2013.

[87] S. S. Groothuis, G. Rusticelli, A. Zucchelli, S. Stramigioli, and R. Carloni, "The variable stiffness actuator vsaut-ii: Mechanical design, modeling, and identification," *IEEE/ASME transactions on mechatronics*, vol. 19, no. 2, pp. 589–597, 2014.

[88] A. Jafari, N. G. Tsagarakis, I. Sardellitti, and D. G. Caldwell, "A new actuator with adjustable stiffness based on a variable ratio lever mechanism," *IEEE/ASME Transactions on Mechatronics*, vol. 19, no. 1, pp. 55–63, 2014.

[89] M. I. Awad, D. Gan, M. Cempini, M. Cortese, N. Vitiello, J. Dias, P. Dario, and L. Seneviratne, "Modeling, design & characterization of a novel passive variable stiffness joint (pvsj)," in *Intelligent Robots and Systems (IROS), 2016 IEEE/RSJ International Conference on*, pp. 323–329, IEEE, 2016.

[90] J.-P. Merlet, *Parallel robots*, vol. 128. Springer Science & Business Media, 2006.

[91] V. Varadharajan, R. Klatzky, B. Unger, R. Swendsen, and R. Hollis, "Haptic rendering and psychophysical evaluation of a virtual three-dimensional helical spring," in *Haptic interfaces for virtual environment and teleoperator systems, 2008. haptics 2008. symposium on*, pp. 57–64, IEEE, 2008.

[92] X. Pei, J. Yu, G. Zong, and S. Bi, "An effective pseudo-rigid-body method for beam-based compliant mechanisms," *Precision Engineering*, vol. 34, no. 3, pp. 634–639, 2010.

[93] M. Taher and A. Saif, "On tunable bistable mems - theory and experiment," *Journal of Microelectromechanical Systems*, vol. 9, no. 2, pp. 158–170, 2000.

[94] B. Vanderborght, R. Van Ham, D. Lefeber, T. G. Sugar, and K. W. Hollander, "Comparison of Mechanical Design and Energy Consumption of Adaptable, Passive-compliant Actuators," *The International Journal of Robotics Research*, vol. 28, no. 1, pp. 90–103, 2009.

[95] B. Siciliano and O. Khatib, *Springer Handbook of Robotics*. Secaucus, NJ, USA: Springer-Verlag New York, Inc., 2007.

[96] J. Arosoki, J. Surakka, T. Ojala, P. Kolari, and J. Jurvelin, "Feasibility of the use of a novel soft tissue stiffness meter," *Physiological Measurement*, vol. 26, no. 3, pp. 215–228, 2005.

[97] S. Mckinley, A. Garg, S. Sen, R. Kapadia, A. Murali, K. Nichols, S. Lim, S. Patil, and P. Abbeel, "Tele-impedance control of a variable stiffness prosthetic hand," in *IEEE International Conference on Robotics and Biomimetics*, pp. 1576–1582, 2012.